NUMERICAL STUDY OF THE OCCURRENCE OF ADIABATIC SHEAR BANDING WITHOUT MATERIAL FAILURE

A Thesis by

Palanivel Swaminathan

Bachelors of Engineering, Anna University, India, 2006

Submitted to the Department of Industrial and Manufacturing Engineering
and the faculty of the Graduate School of
Wichita State University
in partial fulfillment of
the requirements for the degree of
Master of Science

December 2010

© Copyright 2010 by Palanivel Swaminathan

All Rights Reserved

NUMERICAL STUDY OF THE OCCURRENCE OF ADIABATIC SHEAR BANDING WITHOUT MATERIAL FAILURE

The following faculty have examined the final copy of this thesis for form and content, and recommend that it be accepted in partial fulfillment of the requirement for the degree of Master of Science with a major in Industrial Engineering.

_____
Vis Madhavan, Committee Chair

_____
Krishna Krishnan, Committee Member

_____
Ramazan Asmatulu, Committee Member

Accepted for the College of Engineering

_____
Zulma Toro-Ramos, Dean

Accepted for the Graduate School

_____
J. David McDonald, Dean

DEDICATION

To my beloved parents and all my loved ones

ACKNOWLEDGMENTS

I am heartily thankful for the continuous support and guidance by my advisor, Vis Madhavan, throughout my MS studies. He continually motivated in regard to research and my development.

I am thankful for support from NSF (grant #0621174, Program Manager George Hazelrigg) during a portion of my MS studies.

I am gratified to Kiran Srinivasan, Amit Deshpande, Ranjithkumar Krishnamurthi and Ramprasad Venkataraju for their support and encouragement. I would also take this opportunity to thank all my research colleagues and whomsoever I have worked with.

ABSTRACT

Segmented chips that arise as a result of formation of adiabatic shear bands are common in high-speed machining of harder alloys. Analytical models describing the mechanics of segmented chip formation have been developed, and these models do not assume or require failure in the material. Most of the finite element (FE) studies of segmented chip formation in the literature always include failure in the material. This thesis presents a numerical study of the occurrence of adiabatic shear banding without material failure. Here, the mechanical properties of hardened 4340 steel was used as a base line, and Johnson and Cook material model for this material were modified to make the material more prone to shear banding. Simulations were performed in two different commercial FE packages: ABAQUS/Explicit and LS-DYNA. The arbitrary Lagrangian-Eulerian (ALE) approach in ABAQUS/Explicit showed shear banding when mass scaling factor was 100. The same simulation did not show shear banding once the mass scaling was removed. Also, the simulations with accelerated thermal softening kept crashing; likely due to the onset of shear banding causing too much mesh distortion. Since steady state was not achieved with any of these simulations, it is hard to say exactly how the intensity of shear banding changes with material properties.

Finite element studies in the recent literature, where researchers have shown shear banding through strain softening without material failure using the updated Lagrangian approach, were repeated with ALE in ABAQUS. With the reduction in the parameter controlling the curvature based mesh refinement, shear banding has been successfully simulated in ABAQUS. ALE approach in ABAQUS did not produce the same chip geometry shown in literature because the simulations failed since the mesh was not able to reform to

a large extent and produce concave shapes as we see in serrated chips. Mass scaling with a factor of 100 did not affect the result. It should be noted that the strain seems to diffuse with the increase in the element size. So, smaller elements are needed to better capture the strains along the PSZ.

Lagrangian analysis with a parting-layer approach in LS-DYNA showed shear banding for different plastic properties of the material and no shear banding for others. Observations of the effect of different material and mesh parameters on the shear banding intensity have been made from the simulations and future research are proposed.

TABLE OF CONTENTS

Chapter Page

1. INTRODUCTION 1

1.1 Incidence of Shear Bands 1
1.2 Metal Cutting 2
1.3 Objective 2

2. BACKGROUND 4

2.1 Mechanics behind Adiabatic Shear Band Formation 4
2.2 Analytical Models 4
2.3 Numerical studies 5
2.4 Johnson-Cook Material Model 8
2.5 Variation of Plastic Properties and Thermal Conductivity 8

3. ADIABATIC SHEAR BANDING BY ALE APPROACH 9

3.1 Finite Element Model 9
3.2 Material Model 11
3.3 Process of Shear Banding 12
3.4 Results—Other Approaches 16
3.5 Material Model from Literature 18
3.5.1 Results 20
3.5.2 Data Processing: Shear Band Intensity 21
3.5.3 Data Processing: Shear Band Intensity 22
3.5.4 Accuracy of the analysis 23
3.5.4.1 KE/IE Ratio 23
3.5.4.2 Comparison of Flow Stress and Temperature 24
3.5.4.3 Cost of the analysis and Adaptive remeshing 26
3.5.4.4 Mesh Dependency 28
3.5.5 Parametric studies 29
3.5.6 Comparison of Results 30

4. ADIABATIC SHEAR BANDING BY LAGRANGIAN APPROACH 32

4.1 Finite Element Model 32
4.2 Process of Shear Banding 33
4.3 Data Processing: Shear Band Spacing 35
4.4 Results and Discussion 36
4.5 Effect of Cutting Condition Parameters 37
4.5.1 Effect of Depth of Cut 37
4.5.2 Effect of Length of Work Piece and Elastic Tool 38
4.5.3 Effect of Friction 39

4.5.4 Effect of Work Hardening 40
4.5.5 Effect of Thermal Softening 40
4.5.6 Effect of Melting Temperature 41

5. CONCLUSIONS AND FUTURE WORK 43

5.1 Conclusions 43
5.1.1 Simulations results from ABAQUS 43
5.1.2 Simulations results from LS Dyna 44
5.2 Future Work 44

BIBLIOGRAPHY 46

LIST OF TABLES

Table Page

1. Modified Johnson-Cook Constants 11
2. Ozel's Material Model Constants 18
3. Variation of Adaptive Mesh Controls to study the robustness of the simulation 27
4. Cutting Conditions 37

LIST OF FIGURES

Figure Page

1. Schematic sketch of orthogonal cutting showing primary and secondary shear zones 2
2. Initial and finalized chip geometry: 10
3. Flow curve for material with JC and user constants for 4340 steel 12
4. User material flow curve exhibiting strain hardening followed by thermal softening ... 12
5. Flow stress in the material at steady state condition 13
6. Sequence of ten images showing plots of effective plastic strain and change in shear plane angle between one formed band to next 15
7. Plastic strain plot for the simulation with velocity scaling 16
8. Von-mises stress at second step of analysis for first change in value of m 17
9. Flow curve for Ti-6Al-4V 19
10. Sequence of eight images showing plots of effective plastic strain and change in shear plane angle between one formed band to next 20
11. Plastic strain in the material at the end of the analysis 21
12. Plastic strain along the length of the chip 21
13. Flow curve of Ozel – Adiabatic calculation 22
14. Results without the strain softening term in Ozel model 22
15. KE/IE ratio of the analysis 23
16. Mass scaling - Results 24
17. Comparison of FE results with analytical results - Temperature 26
18. Comparison of FE results with analytical results – Flow Stress 26
19. Sensitivity of Curvature Refinement Value 28
20. Mesh Dependency 29
21. Flow curve for different values of M 29
22. Parametric Studies 30
23. Comparison of results 30
24. Finite element model 32
25. Closer view near the tool 33
26. Sequence of ten images showing rate of change of effective plastic strain and change in shear plane angle between one formed band to next 35

27. Plastic strain in the material at steady state condition 36
28. Plastic strain along the length of the chip 36
29. Plastic strain along the length of the chip– Effect of depth of cut 38
30. Shear band spacing—effect of depth of cut 38
31. Plastic strain along length of chip—effect of length of work piece and elastic tool 39
32. Shear band spacing—effect of length of work piece and elastic tool 39
33. Plastic strain along the length of the chip – Effect of friction 39
34. Shear band spacing—effect of friction 39
35. Plastic strain along length of chip—effect of work hardening 40
36. Shear band spacing—effect of work hardening 40
37. Plastic strain along length of chip—effect of thermal softening 41
38. Shear band spacing—effect of thermal softening 41
39. Plastic strain along length of chip—effect of melting temperature 42
40. Shear band spacing—effect of melting temperature 42

LIST OF SYMBOLS

σ	Flow Stress
ε	Strain
$\bar{\varepsilon}^{p^n}$	Effective Plastic Strain
$\dot{\varepsilon}$	Plastic Strain Rate
$\dot{\varepsilon}_0$	Reference Strain Rate = 0.000001/s
T_r	Room Temperature
T_m	Melting Temperature
A	Initial Yield stress
B	Hardening Modulus
n	Work-Hardening Exponent
C	Strain-Rate-Dependent Coefficient
m	Thermal-Softening Coefficient
$\Delta\bar{\varepsilon}^p$	Increment of equivalent plastic strain
ε^f	Strain at Fracture
$D_{i,\ 1\leq i\leq 5}$	Damage Constants
τ	Shear Stress
θ	Temperature

CHAPTER 1

INTRODUCTION

An adiabatic shear band is a mode of failure in metals and alloys due to large shearing when subjected to higher loads. This band is formed by relative displacement of regions as in the in-plane shear or out-of-plane shear modes of failure that achieve strains greater than one ($\varepsilon > 1$) (Recht 1964). The bands are formed due to the sudden drop in the strength of the material due to the increase in temperature which overtakes the work hardening effect that tends to increase the strength of the material. As the name "adiabatic" suggests, the heat generated is retained in the zone itself. The hardness of the metal increases along the shear band due to heating and work-hardening behavior. Because of the large strains encountered in this failure, the grains along the shear band are refined relative to the other regions of the metal, forming a band-like structure. The thickness of the bands formed by this mode of failure measures between 2 μm and 10μm (Recht 1964).

1.1 Incidence of Shear Bands

Adiabatic shear bands occur under various circumstances where the work piece material undergoes intense shear strains and strain rates. Ballistic impacts, torsion Hopkinson bar tests, and industrial processes like machining, forging, drilling, cutting, and shearing are some examples where the strain and strain rates are high and thereby the chance of adiabatic shear band occurrence is high. Since metal cutting is already in widespread use with the availability of analytical models and the ability to attain high strain rates higher by one or two orders of magnitude over the Hopkinson bar and other industrial processes, it naturally becomes a choice to study the formation of adiabatic shear bands.

1.2 Metal Cutting

Metal cutting is the process of removing unwanted material from the surface of a softer work piece with a sharp wedge-shaped rigid tool. The cutting action of the tool causes the work piece to undergo a strain greater than one ($\varepsilon > 1$) over a narrow deformation zone, the thickness of which is up to a few hundredths of a millimeter, which is called the primary shear zone (PSZ), as shown in Figure 1. The cutting speed typically ranges from 0.1 m/s to 100 m/s. The rapid movement of the tool against the work piece at high speeds and the large deformations encountered result in strain rates between 10^3/s and 10^6/s.

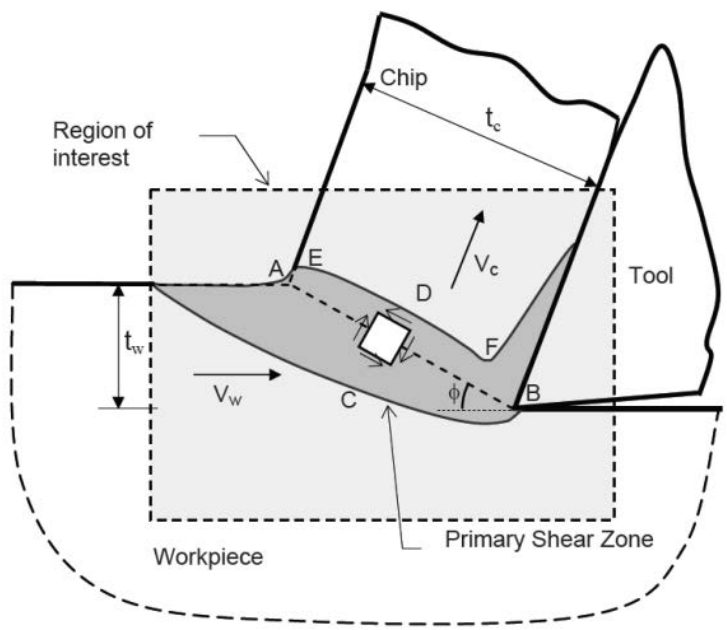

Figure 1: Schematic sketch of orthogonal cutting showing primary and secondary shear zones

1.3 Objective

This thesis describes an approach to simulating shear banding by assuming that no damage occurs in the material and that the chip segmentation is purely adiabatic. The flow stress of the material following the Johnson-Cook (JC) material law is altered by varying the

plastic properties and assuming that the strain rate is linear, where there is no thermal conductivity between the tool and the work piece, and the heat generation is purely due to plastic deformation.

In metal cutting, shear bands can form and reform continuously along the chip. As mentioned earlier, the heat generated during the process is retained along the band itself, and the movement of the chip along the rake surface of the tool results in a moving heat source. This subjects the tool to thermal fatigue, which leads to failure. Also, serrated chips affect the quality of the surface finish and lessening the overall quality of the part. Since metal cutting is used worldwide, a small improvement in the process would mean a large cost savings for industries. Therefore, it is important to understand the occurrence of shear bands using finite element (FE) simulations, which are widely employed in the design manufacturing process. These accurate FE simulations aid in the proper design of machining processes for manufacturing industries.

CHAPTER 2

BACKGROUND

2.1 Mechanics behind Adiabatic Shear Band Formation

The mechanics behind the adiabatic shear band formulation is simple to understand. As plastic deformation sets in during machining, the isothermal flow stress of the metal increases due to the work hardening and strain-rate hardening nature of the material. At the same time, the plastic work is also converted into heat, and this increase in temperature decreases the flow stress. As the cutting progresses, the temperature in the material increases and ends up softening the metal by overtaking the work hardening. Finally, the material becomes weak locally along the PSZ from the tool tip to the free surface. This process is called localization. Once this value is reached, the chip segment is pushed along the direction of strain, and a new segment is formed.

2.2 Analytical Models

Recht (1964) stated that catastrophic slip occurs when the temperature gradients offset the effects of strain hardening, which will strengthen the material. The criterion for catastrophic slip is (1) which defines shear strength as a function of strain and temperature.

$$0 \leq \frac{\frac{\partial \tau}{\partial \varepsilon}}{-\left(\frac{\partial \tau}{\partial \theta}\frac{d\theta}{d\varepsilon}\right)} \leq 1.0 \tag{1}$$

If this ratio is equal to 1, then the chances of shear banding will be higher. The material will not shear band if the ratio is equal to zero. Note that the analytical model does not account for material failure.

Davies and Burns (2002) found that at higher speeds, plastic deformation occurs at the tool tip and localizes because of the lesser time for the temperature gradient to move into uncut material.

2.3 Numerical studies

The process of metal cutting involves the removal of material along the parting line leaving the uncut material to form a chip. This removal can be reproduced in finite element simulations using fracture criterions.

In metal cutting, the material is subjected to biaxial state of stresses and the following theories would contribute to the failure. Maximum principal stress theory, minimum pressure and maximum principal strain theory. According to maximum principal stress theory, the failure in the material occurs when the maximum principal or the normal stress reaches the limiting value. The minimum pressure theory states that the failure in the material occurs when the minimum pressure strain reaches a limiting value. The maximum principal strain theory states that the failure in the material occurs when the maximum principal strain reaches a limiting value.

In addition to this ductile failure, the element deletion in a finite element analysis can be simulated by time step deletion. The time step size is the time required for a stress wave to propagate from one element to another and it depends upon the characteristic length (minimum of the longest side or the longest diagonal) of the element and the velocity of the sound. If the characteristic length of an element increases, the time step size of that element increases proportionately with length. This means the element is distorted severely and the strain in the element will also be higher. By limiting the time step size, the

highly strained element along the parting line can be deleted from the calculation which will evoke the chip formation.

Fracture in an element can be simulated by the cumulative damage model proposed by Johnson and Cook. In the Johnson-Cook law, failure in the material occurs when $D = \sum \frac{\Delta\bar{\varepsilon}^p}{\varepsilon^f}$ reaches the value of 1. The equivalent strain increment is represented by $\Delta\bar{\varepsilon}^p$, and the failure strain ε^f can be calculated using

$$\varepsilon^f = [D_1 + D_2 \exp D_3 \sigma^*][1 + D_4 \ ln \ \varepsilon^*][1 + D_5 \left(\frac{T - T_r}{T_m - T_r}\right)] \tag{2}$$

where D1 to D5 are the damage constant parameters obtained experimentally.

Xie et al. (1998) simulated a shear localized chip with a user-defined material model. This user material model is defined using a piecewise curve such that once the flow stress of the material is past the yield stress, it will start to decrease due to the heat generated from friction and severe plastic deformation. The high temperature causes thermal softening in the shear zone stress and will localize in the zone itself. In their simulation, the chip and the work piece were tied together and separated with a "tie-break" criterion. The nodes were set to separate when the nodal strain increased the criterion value due to the cutting action of the tool.

Ng and Aspinwall (2002) used the link element approach with adaptive remeshing to simulate shear banding. Their work piece was modeled into three parts: chip, remaining work piece, and a set of small link elements to connect the chip and work piece. The conditional link elements were removed from calculation when the cumulative damage value "D" reached 1 in these elements, due to the cutting action of the tool and the formation of a chip.

Belhadi et al. (2005), Guo and Wen (2004), and Duan et al. (2009) simulated the chip formation on 4340 steel using the Johnson-Cook damage parameters along with the adaptive remeshing technique to improve the mesh as the result of huge distortion from the plastic deformation. Belhadi et al. (2005) in their simulation assumed that the calculation is adiabatic and neglected thermal conductivity between the tool and work piece. Guo and Wen (2005) simulated shear banding by using the stagnation effect. The material that stagnates at a point where the material flow is separated as chip and machined surface is deleted when the cumulative damage law criterion is met (i. e., D = 1).

Uhlmann et al. (2007) simulated shear banding in ABAQUS and DEFORM and compared the results with their experiments. Continuous chips were seen with lower cutting speeds like 100 m/min and 200 m/min. Segmented chips were seen starting from a cutting speed 400 m/min up to 1,000 m/min. Aurich and Bil (2006) simulated segmented three-dimensional (3D) chip formation using both thermal softening and the crack propagation approach. They employed Rhim's material model, which softens the material thermally once the melting temperature reaches 0.5 Tm. For the crack propagation approach, they used the Cockroft-Latham damage model, which initiates crack in the PSZ at higher strains and then welds together the failed elements immediately after fracture due to compression and high chemical activity.

Ozel and Sima (2010) and Karpat (2010), in their simulations, showed the formation of shear bands by thermal softening. They included the effects of strain rate and temperature as well as strain and strain rate along with thermal softening at higher strains. Using the updated Lagrangian formulation and remeshing procedures and varying the

thermal softening parameter, they obtained results closer to the experimental observations.

2.4 Johnson-Cook Material Model

In machining, a material undergoes unrecoverable deformations due to high strain and strain rates. Since the process is highly dynamic, and dependent on strain, strain rate and temperature, the material model should be able to compute the flow stress accounting for those parameters.

Johnson and Cook (1985) proposed the following equation to calculate the flow stress in machining (3):

$$\sigma = \left(A + B\bar{\varepsilon}^{p^n}\right) + \left(1 + Cln\left(\frac{\dot{\varepsilon}}{\dot{\varepsilon}_0}\right)\right) + \left(1 - \left(\frac{T - T_r}{T_m - T_r}\right)^m\right) \quad (3)$$

2.5 Variation of Plastic Properties and Thermal Conductivity

Bäker et al. (2003) simulated chip segmentation on cutting Ti6Al4V by assuming no crack growth in the model and only adiabatic shearing. He varied the plastic properties of the material by changing the thermal softening parameter, hardening exponent in Johnson and Cook material model, and thermal conductivity independently in his simulations. The flow stress plots showed a steep decline for the smaller value of all of the above parameters, which indicates the formation of shear bands. With the increase in the value of the above parameters, the frequency of the shear bands decreased as can be seen from the flow stress plots.

CHAPTER 3

ADIABATIC SHEAR BANDING BY ALE APPROACH

This section presents the numerical study where the physical interaction between the tool and the work piece was studied during the cutting action. The aim here was to determine whether shear banding could be simulated by assuming that no damage occurs in the chip material due to the cutting action of the tool and by modifying the original properties of 4340 steel at 18 HRC.

3.1 Finite Element Model

A two-dimensional (2D) coupled thermo-mechanical finite element analysis of orthogonal machining was carried out using the arbitrary Lagrangian-Eulerian (ALE) analysis capability available in ABAQUS/Explicit. ALE formulation uses the advantages of both the Lagrangian formulation, where nodes are forced to move with the material, and Eulerian formulation, where material moves through the mesh. This will maintain a high-quality mesh throughout the analysis, even in the presence of severe distortions, which is common in metal-cutting simulations.

The split-operator approach was used in ABAQUS/Explicit to specify the ALE boundary conditions. Here, in Lagrangian steps, the mesh moves with the material, which is followed by advection steps, where the material flows through the mesh. Mesh smoothing is also carried out during the periodic advection steps to maintain a high-quality mesh. In addition to the advection steps, ABAQUS uses adaptive mesh refinement to maintain the gradient mesh throughout the analysis.

Since the domain of interest is only on the primary and secondary deformation zones, a gradient mesh was used, as shown in Figure 2, to reduce the cost of the analysis. A

typical 2D model consisted of 9,000 2D elements (CPE4RT) for the work piece and 800 elements for the tool.

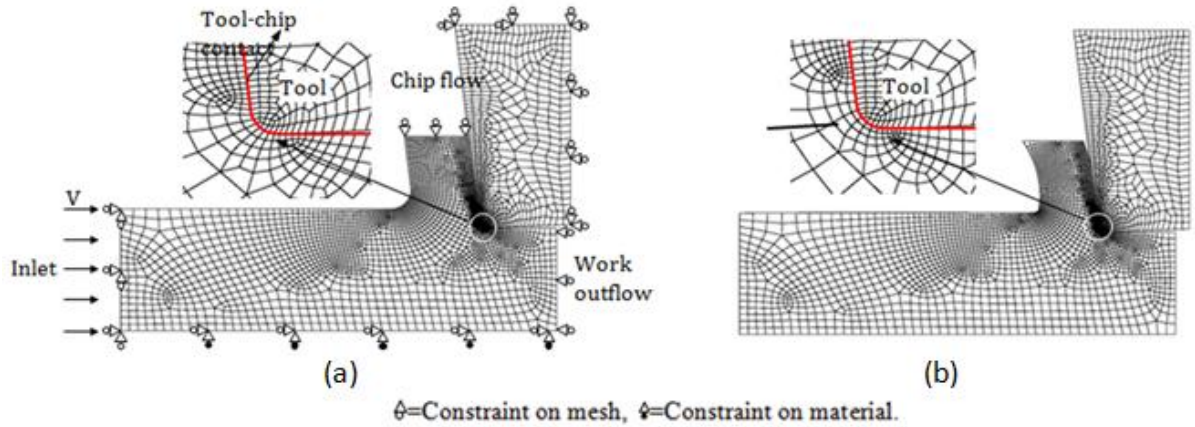

Figure 2: Initial and finalized chip geometry:
(a) initial mesh and boundary conditions, and (b) finalized shape of the chip

The analysis started with an arbitrarily chosen mesh geometry, as shown in Figure 2(a), and the chip geometry was modified automatically as the material flowed through the domain, as shown in Figure 2(b). Further changes in the velocity field with time became insignificant, indicating the initiation of a steady flow pattern after 600 μs.

In the ALE analysis, various constraints were applied along the different boundaries of the work piece. The nodes along the inlet surface (left) of the work piece were constrained in all directions, the bottom nodes (and the material) of the work piece were fixed in the Y direction but free to slide in the X direction, the mesh along the chip top surface (chip outflow) was constrained only in the Y direction, and the mesh along the work outflow surface (back surface) of the work piece was constrained in the X direction. The cutting tool was constrained in all directions along the top and back surfaces, as shown in Figure 2(a).

The work piece material was pushed with an inflow velocity equal to the cutting velocity into the domain of interest (mesh) across the inlet surface and it flowed out of the domain across the work outflow surface and chip outflow surface. A chip-tool penalty contact interface with Coulomb friction was specified between the rake, flank, and cutting edge of the tool. The tool surface acted as the master surface, and the corresponding faces of the work piece acted as the slave surface.

3.2 Material Model

In this investigation, a user material model was used to exhibit strain hardening followed by strain softening due to thermal softening.

Since the machining process is highly dynamic and involves huge strains, strain rates, and temperatures, the material model should also be able to compute the flow stress accounting for those parameters. Assuming the material follows the Johnson-Cook material model, user constants for this model were computed using MAPLE and are shown in Table 1. With the assumption that the strain rate effects were less, the JC constants were modified by trial and error until a flow curve exhibiting the strain hardening followed by thermal softening was achieved (Figure 3). The starting values of JC constants of 4340 steel at 18 HRC were taken from the work of Johnson and Cook (1984). Table 1 shows the modified values of the 4340 steel.

Table 1 Modified Johnson-Cook Constants

	***A* (MPa)**	***B* (MPa)**	***c***	***n***	***m***	***Tm* (deg C)**	***Cp* (J/kg-°C)**
Original JC Constants	792	510	0.014	0.26	1.03	1520	477
User JC Constants	226	792	1e-7	0.30	0.30	400	175

Figure 4 shows the user flow curve for 4340 steel. Point 1 in the flow curve is the yield strength of the material. When the material reaches this point, it enters into the plastic zone. From point 1 to point 2, the material will harden as the strain increases. The increase in strain will also increase the flow stress. After point 2, due to plastic deformation and friction due to the tool's cutting action, heat is generated in the primary shear zone. The increase in temperature will cause the material to soften, thus overcoming the strain hardening, and the flow stress will decrease.

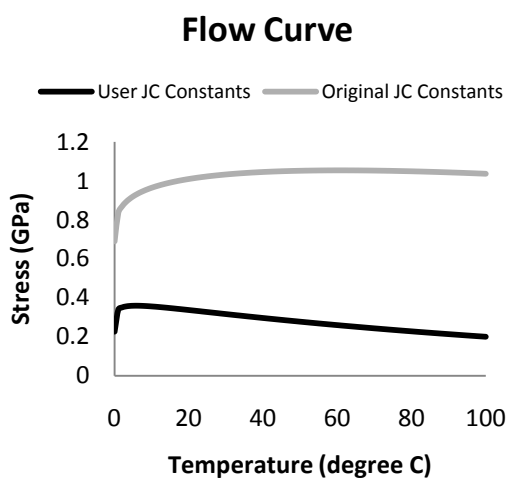

Figure 3: Flow curve for material with JC and user constants for 4340 steel

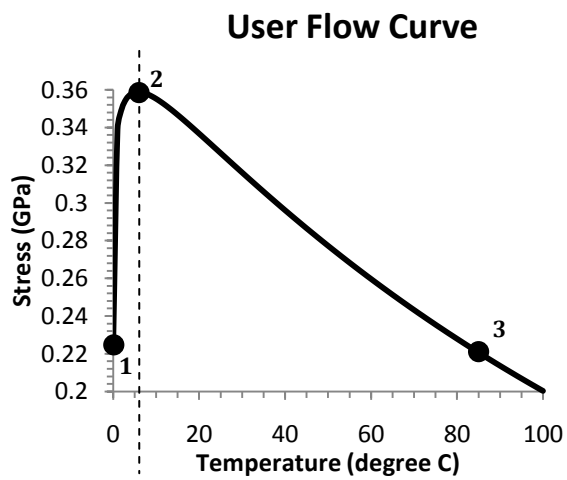

Figure 4: User material flow curve exhibiting strain hardening followed by thermal softening

It is important to note that after reaching point 2 in the curve, the flow stress of the material will drop drastically such that the value is less than the yield stress of the material when the temperature reaches one-quarter of its melting temperature. Therefore, this material model can simulate shear banding in the metal-cutting process.

3.3 Process of Shear Banding

Figure 5 shows the flows stress in the PSZ at the steady-state condition. The cutting conditions were as follows: velocity 30 m/s, depth of cut (DOC) 100 μm, friction between

tool and work piece 0.1 (assumed), tool rake angle 30 degrees, and edge radius 6 μm. The cutting speed was high enough so that conduction from the shear zone was small, which means that most of the heat generated due to plastic deformation stayed in the shear zone. A mass scaling factor of 100 was used to reduce the cost of analysis. Figure 5, shows that the maximum value of the flow stress is 0.44 GPa instead of the computed value 0.36 GPa. This is because the JC parameters were computed by assuming that the strain rate effects were less. Since the strain rates were high in the actual machining, the flow stress was also higher.

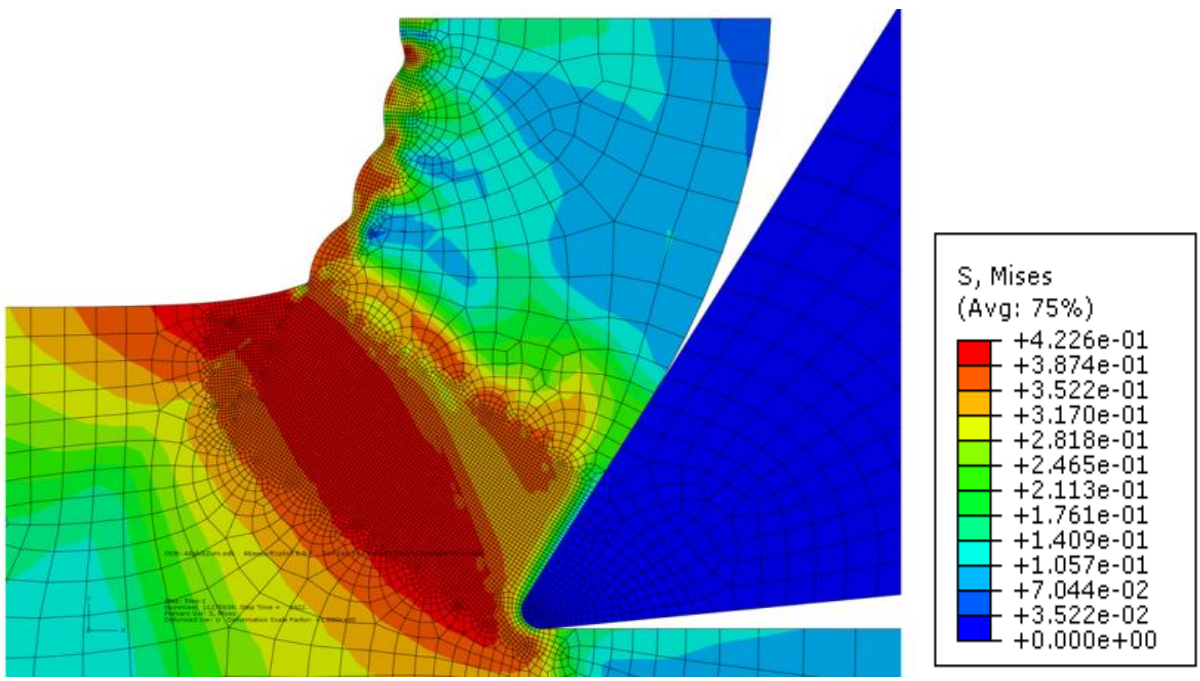

Figure 5: Flow stress in the material at steady state condition

The plots in Figure 6 show the change in the effective plastic strain between the bands during the cutting action of the tool. They also show the change in the shear angle between one formed shear band to the next. Figure 6 (a) shows a completely formed shear band from the tool tip to the free surface of the chip. It should be noted that the band is

narrow along the PSZ. As the tool moves, the band starts to become wider, which is shown in Figure 6 (b) and (c). Figure 6 (d) shows the starting of a new shear plane angle. Then the shear bands follow the new shear plane angle and form the next band, which is shown in the sequence Figure 6 (e) to (j).

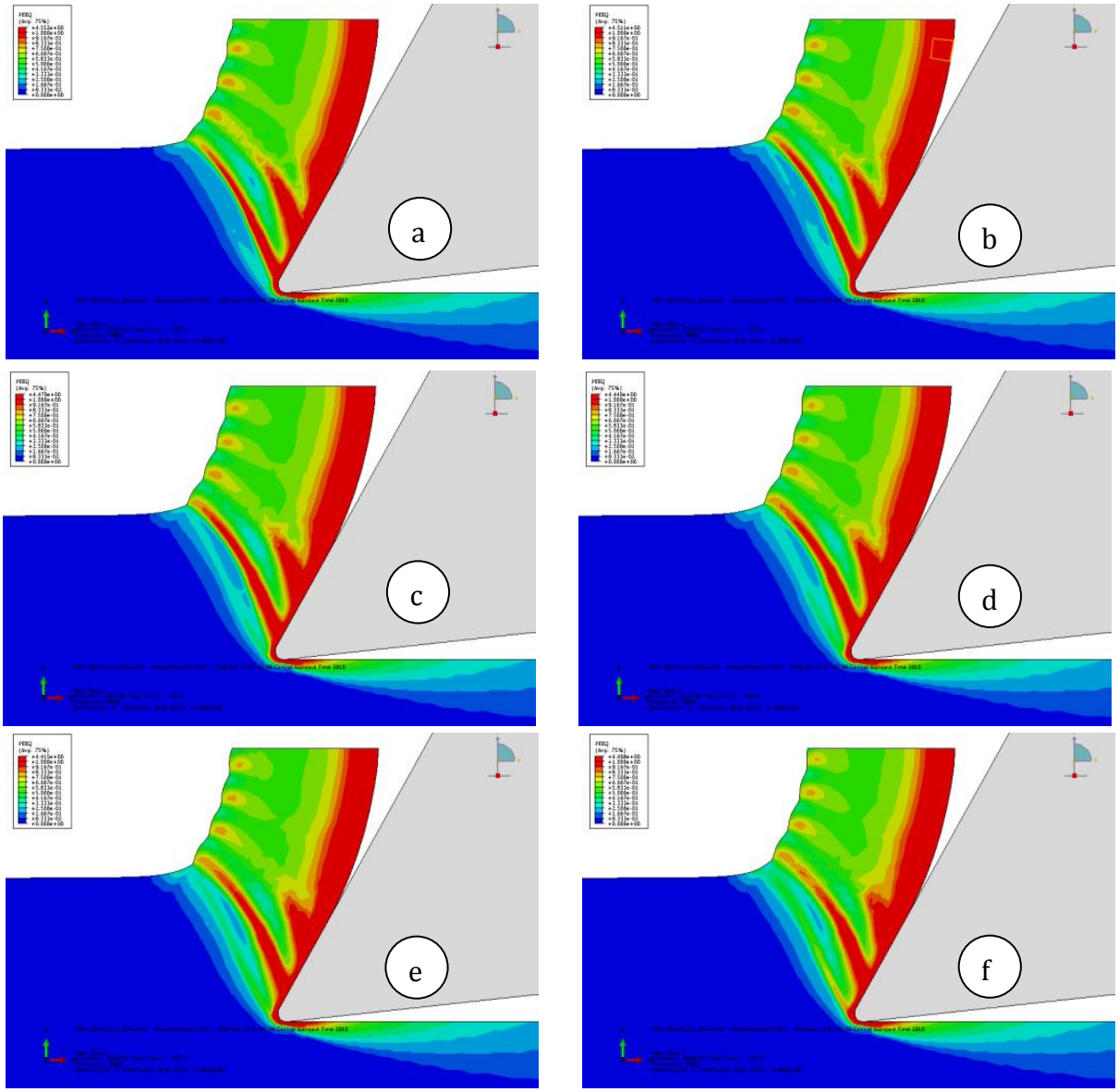

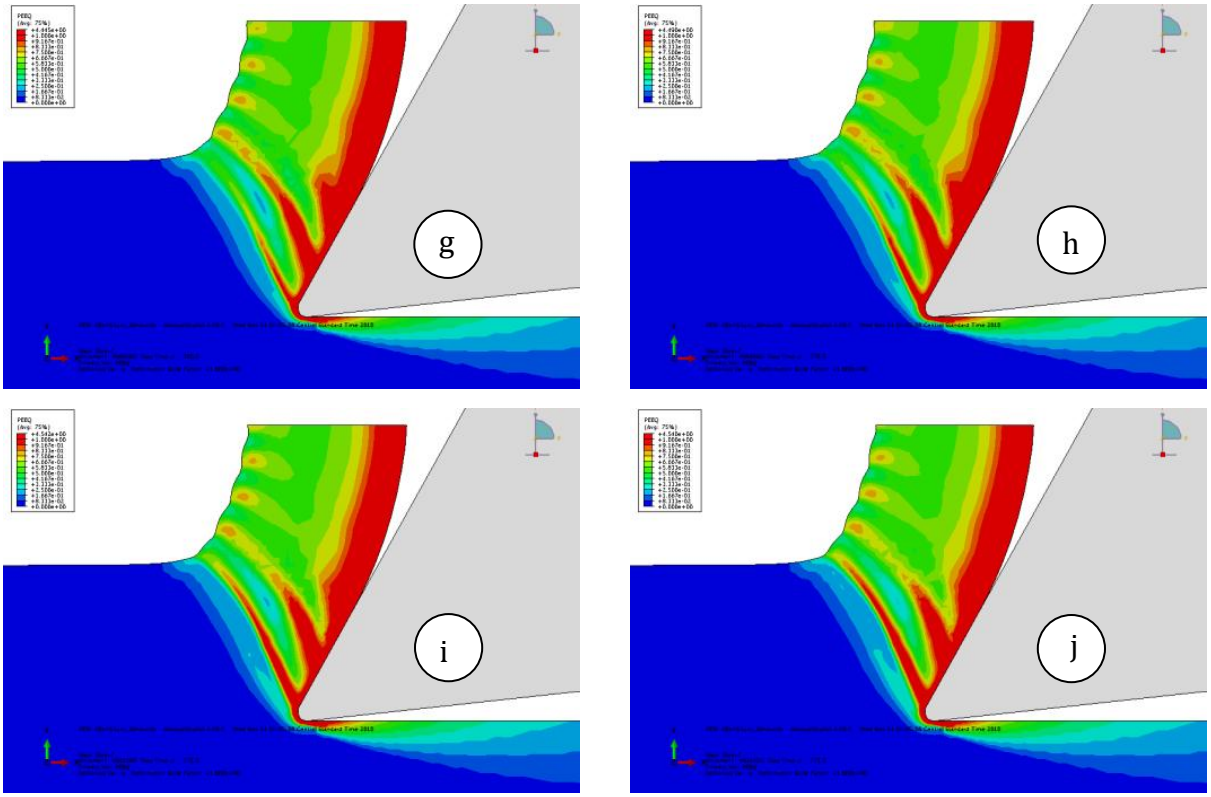

Figure 6: Sequence of ten images showing plots of effective plastic strain and change in shear plane angle between one formed band to next

These results show that under some cutting conditions, the formation of shear bands is evident. The same FE model under the same cutting conditions did not show the occurrence of shear bands when the mass scaling was removed. This indicates that there is some sort of mass effect contributing to the formation of shear bands. To evaluate this, a simulation was done with velocity scaling (10 times) instead of mass scaling. The cutting velocity used was 300 m/s instead of 30 m/s. Since the cutting velocity was high, the strain rate was also high. To simulate the same cutting condition as above, the reference strain rate in the material model was also scaled by 10 times ($\dot{\varepsilon}_0$ = 10). Results of this simulation are shown in Figure 7, which indicates an unusual plot of plastic strain. This is because with the adaptive remeshing and mesh smoothing to adjust the mesh to steady state, the

fine mesh moved upwards, and there was coarser mesh along the PSZ, which diffused the strains. The mesh effect was also significant for the shear band formation.

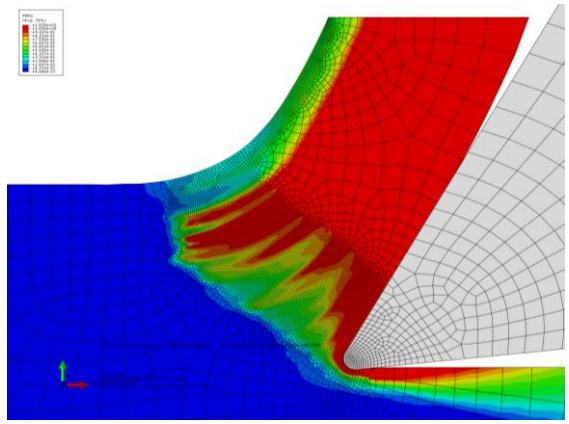

Figure 7: Plastic strain plot for the simulation with velocity scaling

3.4 Results—Other Approaches

The results of adiabatic shear banding using the ALE approach and other approaches are as follows:

- Since no shear banding was seen with the positive rake tool, a negative rake tool was used to increase the strain and promote shear banding.
- No shear banding was seen with the modified properties of 4340 steel and the negative rake tool. This may be due to the large jumps made in the values of the JC parameters to accelerate shear banding.
- Instead of creating large jumps in the JC constants, the simulation was run with the original 4340 steel properties until it reached the steady state. The stress state after the 1,000 μm length of cut was used as the initial condition, and the parameter "m" in the JC model was varied in 0.01 steps to study its response to shear banding.

- The *IMPORT command in ABAQUS/Explicit was used to import the nodal positions, stress, strain, and temperature; and the *INITIAL CONDITIONS, TYPE=VELOCITY command was used to import the velocity.
- Simulations crashed in the first few steps of the analysis due to the loss in temperature and increase in flow stress, as shown in Figure 8.
- The reason for the loss in temperature was because *IMPORT did not support Johnson-Cook plasticity.
- In addition to the above approach, the ALE adaptive meshing parameters, such as adaptive meshing frequency, curvature refinement, mesh constraint angle, mesh sweeps, and mesh smoothing parameters, were changed to capture the shear band formation. As shown in the Figure 8, all simulations failed in the same manner.

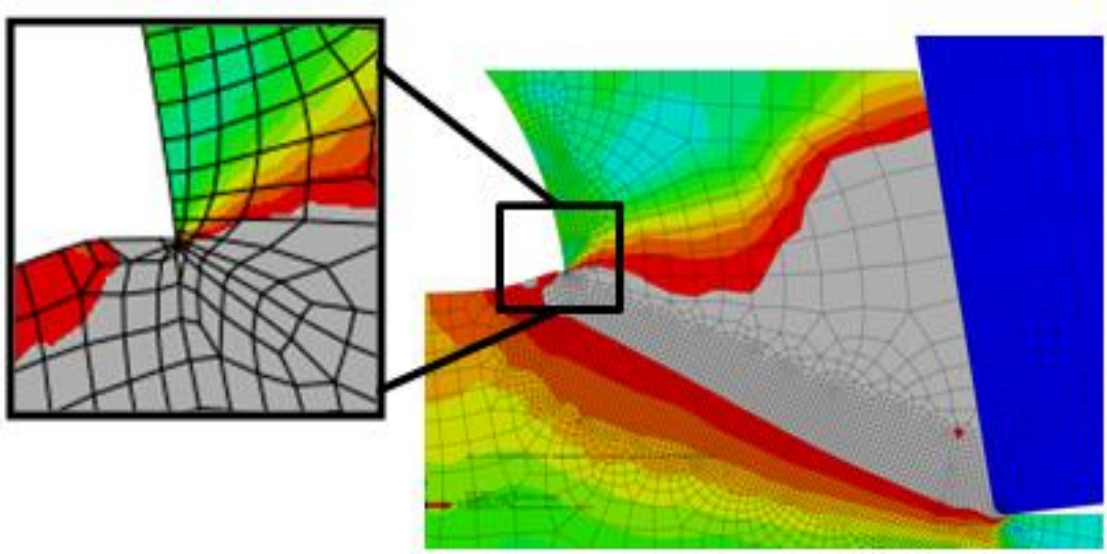

Figure 8: Von-mises stress at second step of analysis for first change in value of m

3.5 Material Model from Literature

Since our user material model did not show shear banding for other cutting conditions, finite element results in literature where the researchers have shown shear banding were performed and the results were compared.

Ozel and Sima (2010) simulated shear banding using updated Lagrangian approach in DEFORM where the chip separation is achieved from continuous remeshing. The work material was Ti-6Al-4V and they employed a strain, strain rate and temperature sensitive material model that includes strain softening effect at higher strains and is given by (4). During strain softening the flow stress will decrease and after a critical value of strain the strain hardening overtakes and continues to increase the flows stress of the material.

$$\sigma = \left(A + B\bar{\varepsilon}^{p^n}\right)\left(1 + Cln\left(\frac{\dot{\varepsilon}}{\dot{\varepsilon_0}}\right)\right)\left(1 - \left(\frac{T-T_r}{T_m-T_r}\right)^m\right)\left(M + (1-M)\, tanh\left(\frac{1}{(\varepsilon+p)^r}\right)^s\right) \quad (4)$$

They have used the experimental flow stress data of Lee and Lin (1998) in their simulations for Ti-6Al-4V (Table 1).

Table 2 Ozel's Material Model Constants

	A (MPa)	***B (MPa)***	***c***	***n***	***m***	***M***	***p***	***r***	***s***	***T_m (deg C)***
Lee and Lin	782.7	498.4	0.028	0.28	1	0.7	0	1	7	1604

The mechanical and thermo physical properties of the material are defined as a function of temperature and are given by (5), (6), (7) and (8)

$$E\,(T) = 0.7412*T + 113375 \text{ [MPa]} \quad (5)$$

$$\alpha\,(T) = 3e\text{-}9*T + 7e\text{-}6 \text{ [mm.mm}^{-1}\text{.°C}^{-1}\text{]} \quad (6)$$

$$\lambda\,(T) = 7.039e^{0.0011*T} \text{ [W.m}^{-1}\text{. °C}^{-1}\text{]} \quad (7)$$

$$\rho Cp\,(T) = 2.24e^{0.0007*T} \text{ [N.mm}^{-2}\text{. °C}^{-1}\text{]} \quad (8)$$

Figure 9 shows the flow curve for the material model (4) under different strain rates. Note that, the flow stress drops at a strain of 0.5 and then continues to increase due to strain hardening after a strain of 1. The parameter M determines the strain at localization.

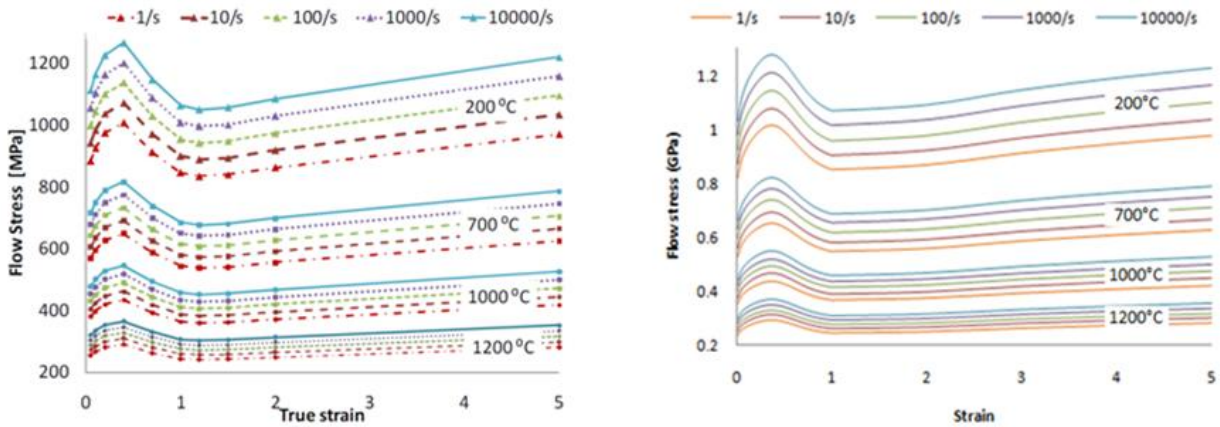

a. Flow curve from Ozel's paper

b. Flow curve reproduced from Ozel's material model

Figure 9: Flow curve for Ti-6Al-4V

The material model above is implemented in ABAQUS/Explicit using ALE approach for the cutting condition shown in the literature: cutting velocity = 2m/s; depth of cut = 75μm; friction between tool and the workpiece = 1.0; tool rake angle = 0° and tool nose radius = 5μm.

In ALE, the steady state chip geometry is very much different from the starting chip geometry. Since the friction coefficient is 1.0, the starting chip thickness should be wider and as the cutting progresses the chip thickness will start to reduce with the increase in temperature and the reduction in the flow stress. Since there is a chance for the simulation to fail during the remeshing steps to accommodate the chip geometry, the friction in the FE model is increased from 0 to 1 for every 10μs with an increment of 0.1.

3.5.1 Results

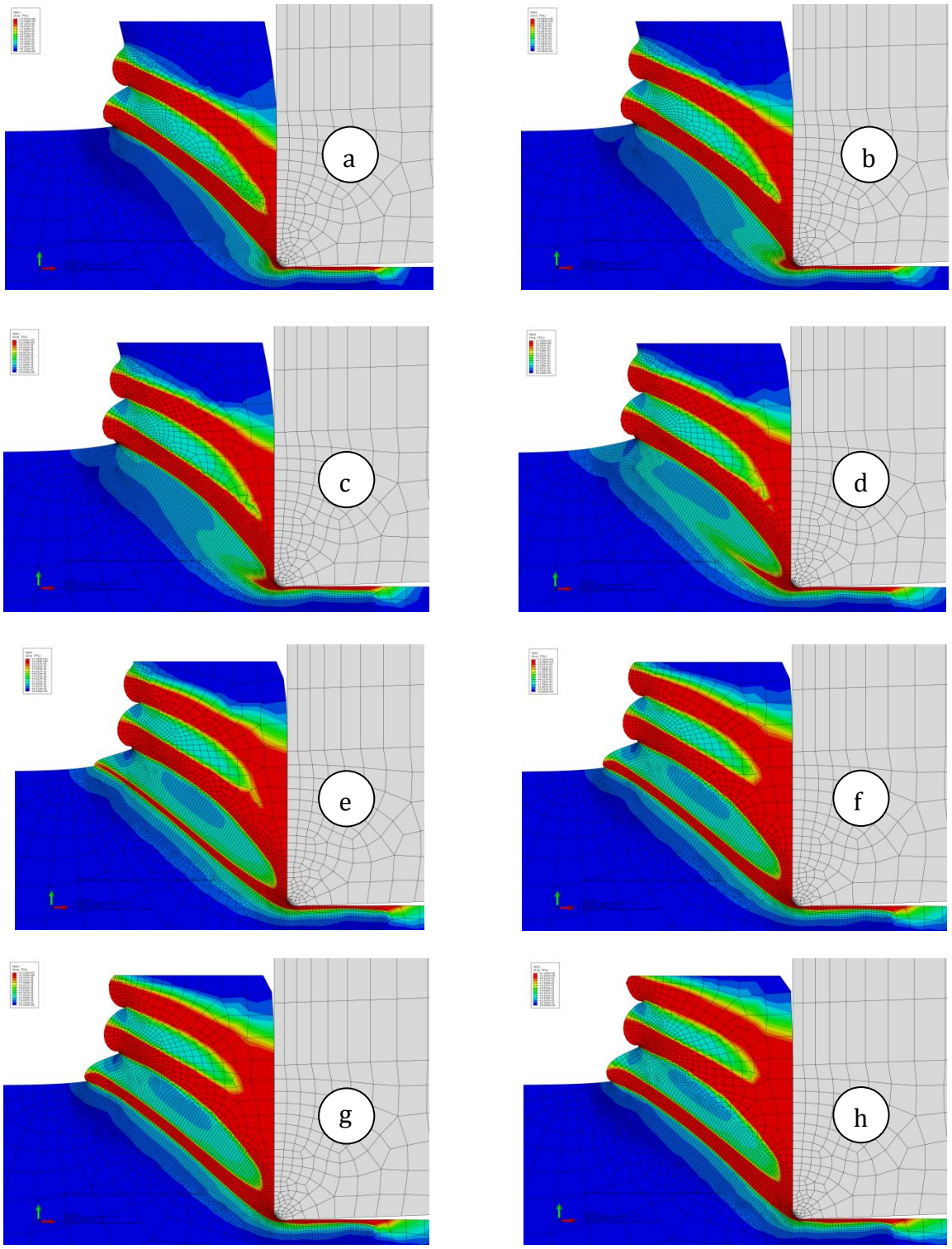

Figure 10: Sequence of eight images showing plots of effective plastic strain and change in shear plane angle between one formed band to next

3.5.2 Data Processing: Shear Band Intensity

Shear bands can be characterized by the strain values along the length of the chip. Figure 27 shows the plastic strain plot at the end of the analysis (analysis crashed after forming three bands). The strain data was extracted along the CD direction starting from the PSZ up to 10 shear bands or 200 μm along the length of the chip. Enough data points were collected along the line so that strain values along the length of the chip were not overlooked. Figure 28 shows the plastic strain data along the length of the chip. The strain is zero below the PSZ, which corresponds to point 1 in Figure 27. Shear band intensity can be measured by the ratio of maximum strain to the average strain.

From Figure 28 it can be seen that the peak strain varies as we move from PSZ to the end of the chip. This can be due to two reasons. First reason was that the increase in friction with the increments of 0.1 for every 10μs. This will in turn increase the chip thickness and the strain along SSZ. The second reason was that the increase in the element size after PSZ diffuses the strain. Due to this reason, only the strain in the last band is considered for calculation. The shear banding intensity for this simulation is 4.0.

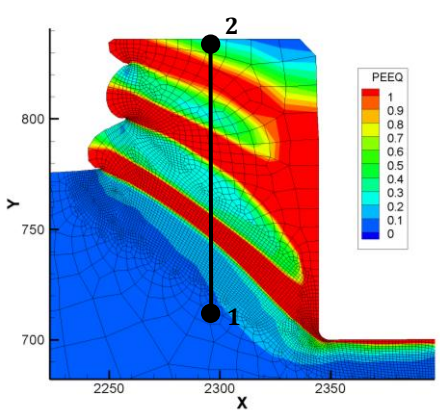

Figure 11: Plastic strain in the material at the end of the analysis

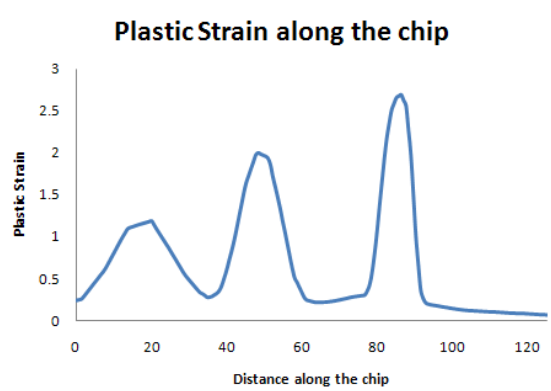

Figure 12: Plastic strain along the length of the chip

3.5.3 Data Processing: Shear Band Intensity

The strain softening term in (3) corresponds to the steep decrease in the flow stress. Figure 13 shows the flow curve for the Ozel model solved adiabatically using the maple code we generated. It also shows the flow curve for the model without the strain softening parameter. It should be noted that the flow stress decreases rapidly after a strain of 0.5. The reduction in the flow stress was uniform without the strain softening parameter and in that case the flow stress equation is same as that of Johnson and Cook.

With the removal of the strain softening term in the flow stress equation, the strains in the chip were lesser as shown in the Figure 14. The shear banding intensity for this simulation was 1.69.

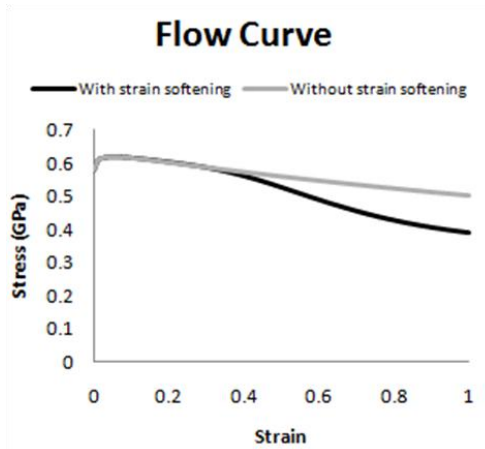

Figure 13: Flow curve of Ozel – Adiabatic calculation

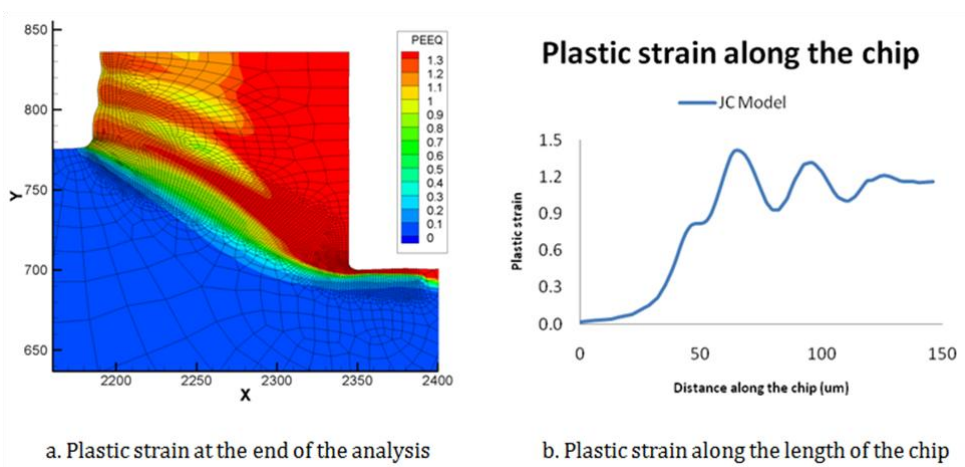

a. Plastic strain at the end of the analysis

b. Plastic strain along the length of the chip

Figure 14: Results without the strain softening term in Ozel model

3.5.4 Accuracy of the analysis

3.5.4.1 KE/IE Ratio

In explicit analysis, the time step of an element is very small to maintain numerical stability. The cost of the analysis will depend upon the element time step. If the time step size of an element is small, the cost of the analysis will be more. To overcome this, non-physical mass is added to the elements to achieve larger time step which will in turn reduce the cost of the analysis. The structural time step can be increased by scaling the density of the elements by a scale factor. In a coupled thermal analysis, in addition to the structural time step the thermal time step should also be increased to achieve the numerical stability. This can be achieved by scaling the specific heat capacity by a scale factor. The increase in the mass of the elements in a dynamic analysis also increases the acceleration and will result in over prediction of forces (10). If the kinetic energy is very small relative to the peak internal energy then the addition of mass will not affect the results.

$$F = m*a \tag{10}$$

Two simulations were run with one having no mass scaling and another with a mass scaling factor of 100. Figure 15 shows the ratio of the kinetic energy to the peak internal energy for both simulations. The ratio was only 0.1% for the analysis with no mass scaling and 35% for the analysis with mass scaling. This shows that the simulation with no mass scaling can be

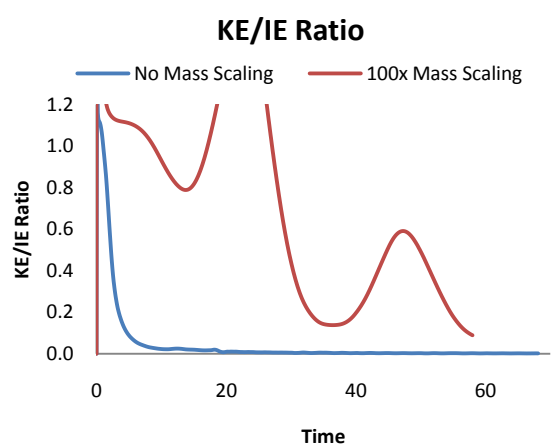

Figure 15: KE/IE ratio of the analysis

trusted since the results are not affected by the inertial effects.

Figure 16 shows the results of the analysis with and without mass scaling. Both the analysis failed after forming three bands. The mode of failure was same for both the analysis except the simulation with 100x mass scaling failed earlier to the other. From Figure 16 (a) and (b), it can be seen that the chip geometry is also different in both the analysis. Figure 16 (c) shows the plastic strain along the length of the chip. The plastic strain pattern seems to be the same for both the analysis.

3.5.4.2 Comparison of Flow Stress and Temperature

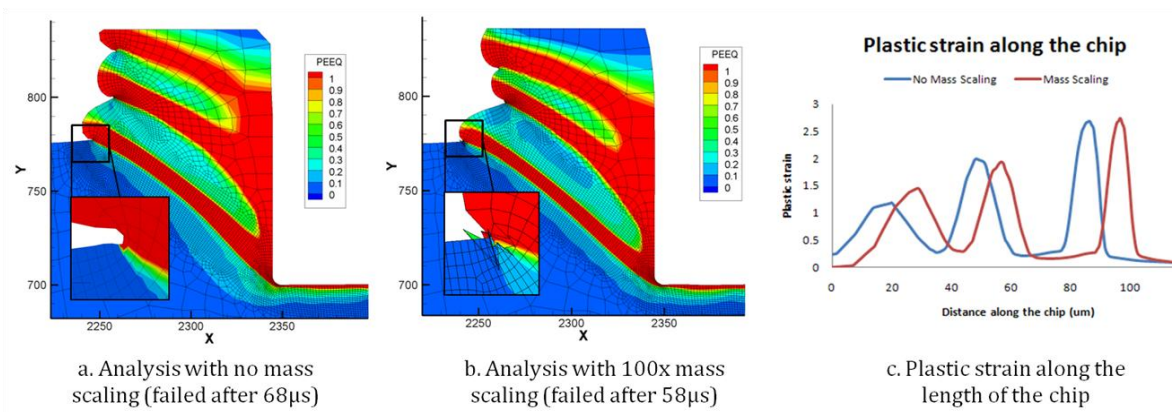

a. Analysis with no mass scaling (failed after 68μs)

b. Analysis with 100x mass scaling (failed after 58μs)

c. Plastic strain along the length of the chip

Figure 16: Mass scaling - Results

After establishing that there are no inertial effects in the simulation, the temperature and flow stress along the free edge of the chip was compared with the analytical calculation to the FE results.

*TRACER PARTICLE is an option in ABAQUS/Explicit where we can define tracer particles typically a set of nodes and assign them to tracer sets (node sets) for tracking the location of and results at material points during a step. This is a better way to write the history outputs at the material points when adaptivity is used. The tracer node set is used along with the *ELEMENT OUTPUT and/or the *NODE OUTPUT options to request output

for the tracer particles. Since the tracer particles are defined as a set of nodes, we can only get U, V, A, and COORD data because of the limitations of *NODE OUTPUT. *ELEMENT OUTPUT requires an element set to write the output variables for that element set. Since the tracer particles are defined as a node set there is no element set to define in *ELEMENT OUTPUT.

Because of this drawback an element along the free edge of the chip was taken for the calculation and using *ELEMENT OUTPUT, HISTORY option, the flow stress (σ), plastic strain (ε) and the temperature (T) of the element was written as a history output. In ALE, we know that the material flows through the element and through *ELEMENT OUTPUT, HISTORY option we will get the history of the material that flown through that element over time. By using (11) the change in temperature (ΔT) is calculated and compared with the FE results.

$$\sigma * \Delta\varepsilon = \Delta T * \rho Cp \tag{11}$$

Figure 17 shows the comparison of the temperature values for the element along the free edge of the chip. It can be seen that the calculated values are 10 times higher than the FE resluts. Since the calculation is adiabatic the.

Figure 18 shows comparison of the flow stress for an element along the free edge of the chip. It can be seen that the flow stress along that element is almost the same.

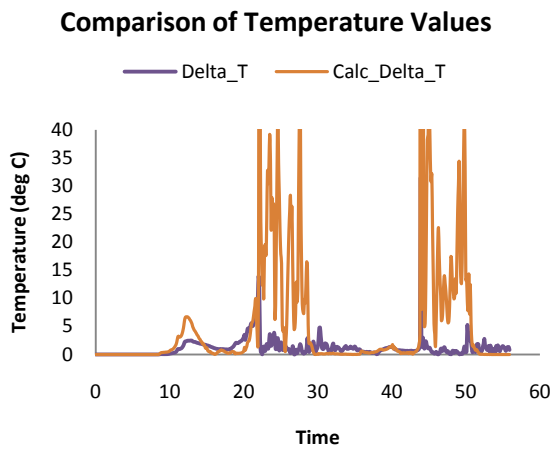

Figure 17: Comparison of FE results with analytical results - Temperature

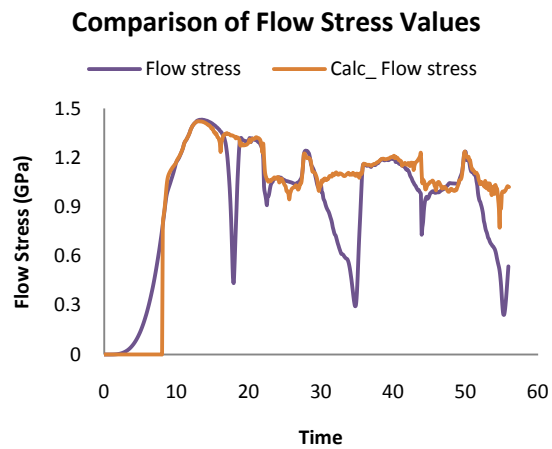

Figure 18: Comparison of FE results with analytical results – Flow Stress

3.5.4.3 Cost of the analysis and Adaptive remeshing

With mass scaling being 1 in the analysis to reduce the inertial effects, the cost of the simulation increased to a great extent. It took 66 hours to form three bands and the analysis failed after forming the third band.

In the process of shear band formation, the mesh has to reform continuously to maintain the shape of the domain. The *ADAPTIVE MESH CONTROL card in ABAQUS/Explicit is responsible for maintaining the shape of the domain when there is severe plastic deformation. The parameters such as curvature refinement, frequency of remeshing and the mesh constraint angle in *ADAPTIVE MESH CONTROL card played a crucial role in the success of the simulation.

In metal cutting simulations where the strain rates are high, the elements will be subjected to deform severely. The strain in these elements will be more and due to further deformation the elements enter into negative volume and the simulation will fail at that point. So the mesh has to be refined frequently in order to maintain the element quality and time step for the numerical stability.

Concave curvatures are common in shear banding simulations. In cases where we have concave curvatures in our model and we depend on solution based meshing for mesh refinement (default in ABAQUS/Explicit), the elements will be pulled towards the area of higher strain to maintain more number of elements and capture the curvature of the boundary. In general, the best practice is to have fine mesh along the curvature and not to depend on solution based mesh refinement. The curvature refinement parameter maintains nominal mesh refinement in the areas where the curvature is at maximum. Lesser the value of curvature refinement indicates no solution dependence to evolving curvature of the boundary.

When the normal to the boundary region approaches the direction of the applied mesh constraint, huge mesh motions will be required to maintain the constraint. To overcome this, ABAQUS terminates the analysis at a prescribed cut-off angle θc. This cut-off angle is referred to as the mesh constraint angle, and its default value is 60°.

Simulations were run for various values for these parameters to find what parameters affect the stability of the analysis. Table 3 shows the results of the analysis. From the table it can be seen that all the simulations were crashed at one point and the simulation that has smallest value for curvature refinement lasted longer.

Table 3 Variation of Adaptive Mesh Controls to study the robustness of the simulation

No	***Frequency***	***Curvature refinement***	***Smoothing objective***	***Meshing predictor***	***Mesh constraint angle***	***Result***
1	8	0.8	GRADED	PREVIOUS	5	Failed after 23μs
2	8	0.1	GRADED	PREVIOUS	5	Failed after 24.5μs
3	8	0.01	GRADED	PREVIOUS	5	Failed after 41.6μs
4	8	0.0001	GRADED	PREVIOUS	5	Failed after 62.3μs
5	1	0.0001	GRADED	PREVIOUS	5	Failed after 44.9μs
6	1	0.0001	GRADED	PREVIOUS	85	Failed after 44.9μs
7	1	0.0001	UNIFORM	CURRENT	85	Failed after 17.8μs
8	8	0.000001	GRADED	PREVIOUS	5	Failed after 41.6μs

Figure 19 show the results of simulation for two different values of curvature refinement. With curvature refinement value of 0.1, the analysis crashed after forming one band (Figure 19 (a)) whereas with 0.0001 the analysis survived a little longer (Figure 19 (b)). From these results, it can be concluded that lesser the value of curvature refinement, higher chances for the survival of the analysis. With further reduction in the value of curvature refinement did not help after 0.000001.

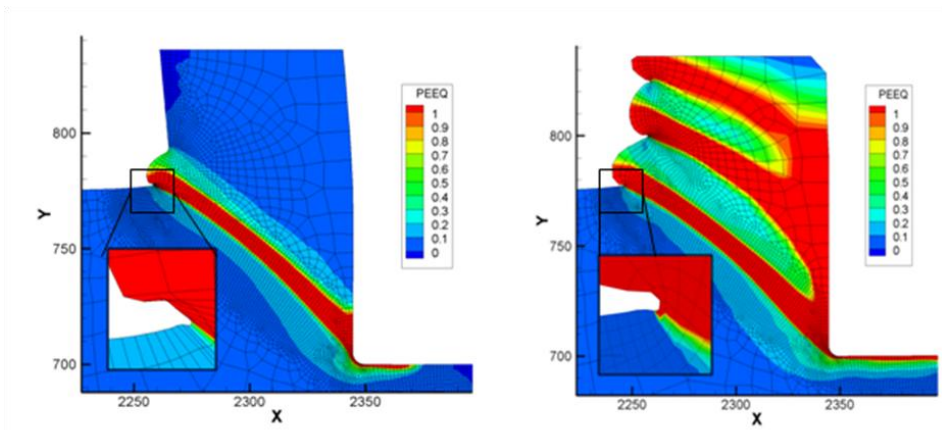

a. Curvature refinement = 0.1 (failed after 24.5μs)

b. Curvature refinement = 0.001 (failed after 68μs)

Figure 19: Sensitivity of Curvature Refinement Value

3.5.4.4 Mesh Dependency

After establishing the accuracy of the analysis, the solution dependency on the mesh size was studied. Two different mesh sizes were compared as shown in the Figure 20. The plot below (Figure 20(c)) shows plastic strain along the chip to study the mesh effect. From the plot we can say that for increase in the mesh size by 4 times reduces the peak strain by two times. (Fine mesh size = 1.5um, peak strain=2.697178; Coarse mesh size = 6um, peak strain = 1.302494). The shear band intensity was 2.89 (average value for 3 bands) for fine mesh and 4.56 for coarse mesh.

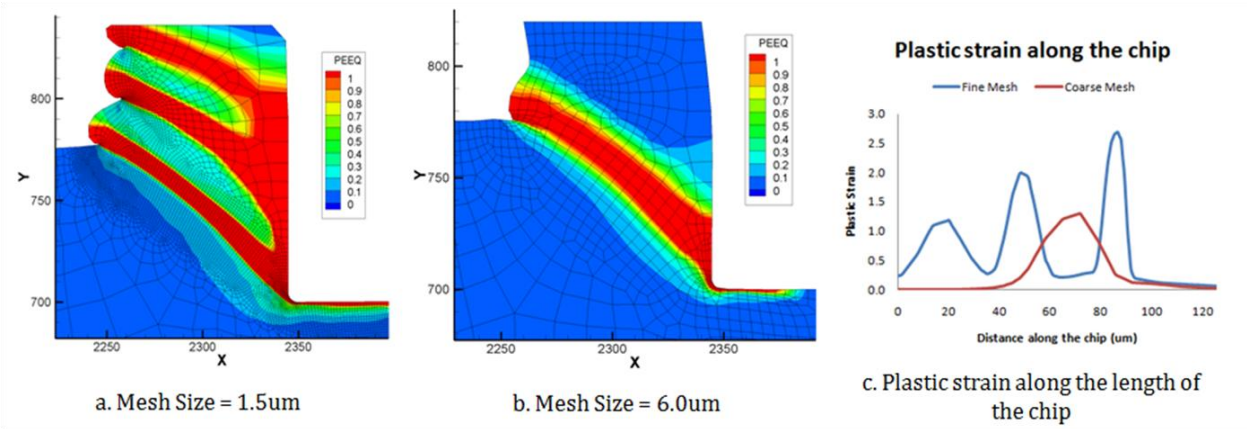

a. Mesh Size = 1.5um

b. Mesh Size = 6.0um

c. Plastic strain along the length of the chip

Figure 20: Mesh Dependency

It is clear from the analysis that the finer mesh size is important to capture the shear banding. Coarser the element size, less accurate the result will be. It should also be noted that further increase in the mesh size would result in a continuous chip.

3.5.5 Parametric studies

The parameter M in (4) substantially modifies the drop in the flow stress. Simulations were run for two different values of M and the results are plotted. Figure 21(a) and (b) shows the flow curve for M=0.8 and M=0.9.

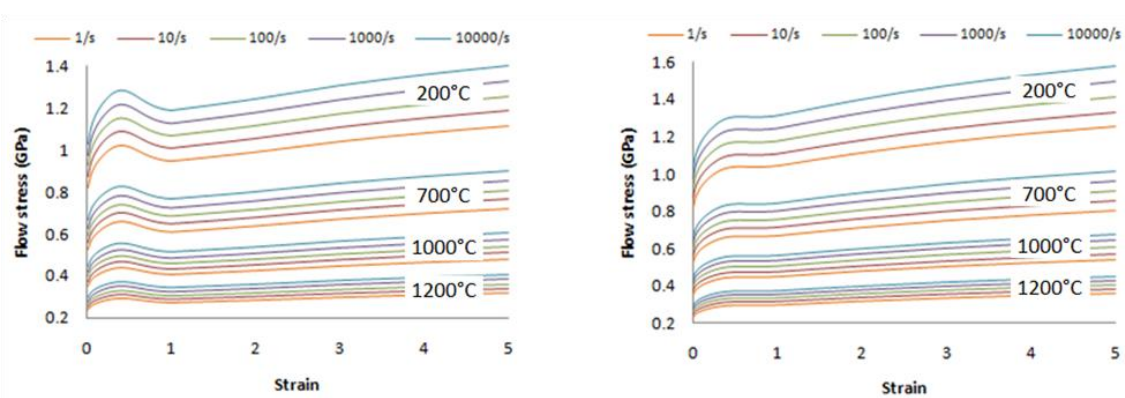

a. Flow curve for M = 0.8

b. Flow curve for M = 0.9

Figure 21: Flow curve for different values of M

From the plots (Figure 21(c)) it can be seen that the as the value of M increases, the peak value of the plastic strain will decrease which means the decrease in the flow stress will be less for higher values of M

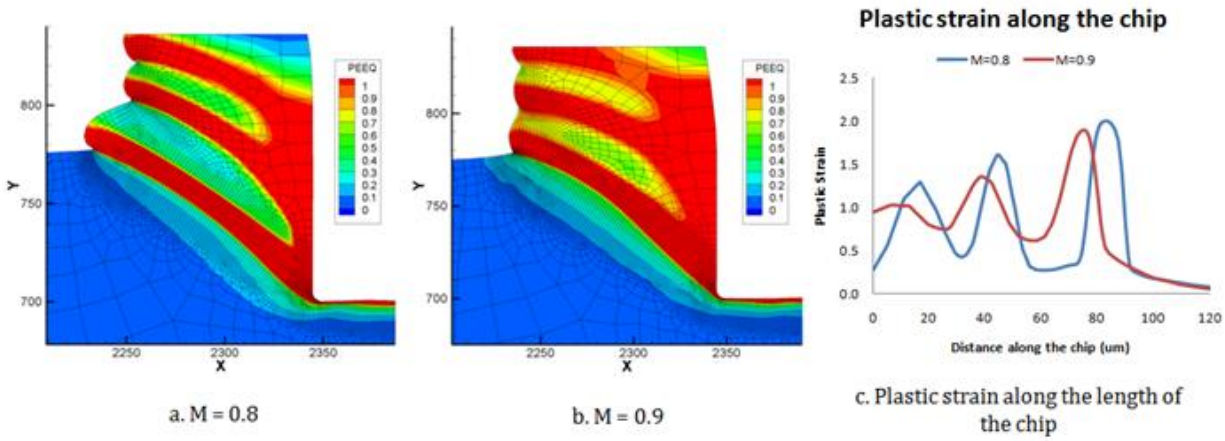

a. M = 0.8

b. M = 0.9

c. Plastic strain along the length of the chip

Figure 22: Parametric Studies

3.5.6 Comparison of Results

Figure 23 shows the comparison of results from literature to the current study. Figure 23(a) shows the result from literature at steady state. Figure 23(b) shows the result from the current study after 60μm of material being cut. The simulation crashed after that step because the ALE mesh was not able to refine due to severe plastic deformation. It can

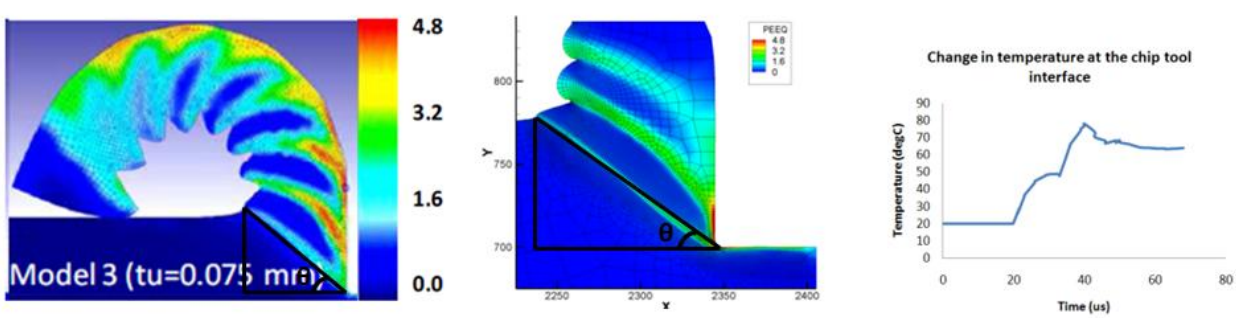

a. Results using updated Lagrangian formulation in DEFORM (Plastic strain plot from literature)

b. Results using ALE formulation in ABAQUS(Plastic strain plot from current study)

c. Change in temperature at the chip tool interface (Result from current study)

Figure 23: Comparison of results

be seen from the plots that the strain values differ because the friction is varied from 0 to 1 over 100μs in the current study whereas the friction was kept constant in the literature. The shear angle was 40° in the literature and 35° in the current simulation. This is also due to the fact that the friction is low and temperature in the tool has not reached steady state (Figure 23(c)).

The adaptive mesh controls parameters used in this analysis are as follows: frequency 1, curvature refinement 0.001, mesh sweeps 4, mesh constraint angle 85 and smoothing objective graded. Also, the literature results show triangular shear band formation where as ALE results show circular band formation. This is because in ALE the mesh couldn't reform much and change its shape to the severe plastic deformation due to the sudden decrease in the flow stress.

This shows ALE cannot be used in places where the plastic deformations are huge. Simulations will result in failure because the mesh will not be able to reform to a large extent and produce concave shapes as we see in serrated chips.

CHAPTER 4

ADIABATIC SHEAR BANDING BY LAGRANGIAN APPROACH

4.1 Finite Element Model

A two-dimensional plane strain adiabatic explicit finite element model of orthogonal machining was used in this work (see Figure 24). The Lagrangian analysis had four noded, fully integrated shell elements. The tool was modeled as rigid with 500 elements, and the work piece had approximately 45,000 elements. The cutting conditions were as follows: cutting velocity 30 m/s, depth of cut 100 μm, friction between tool and work piece 0.1 (assumed), tool rake angle 30 degrees, and a sharp tool. The cutting speed was high enough so that conduction out of the shear zone was small, which meant that most of the heat generated due to plastic deformation stayed in the shear zone itself. The work piece was fixed, and the rigid tool moved against the work piece.

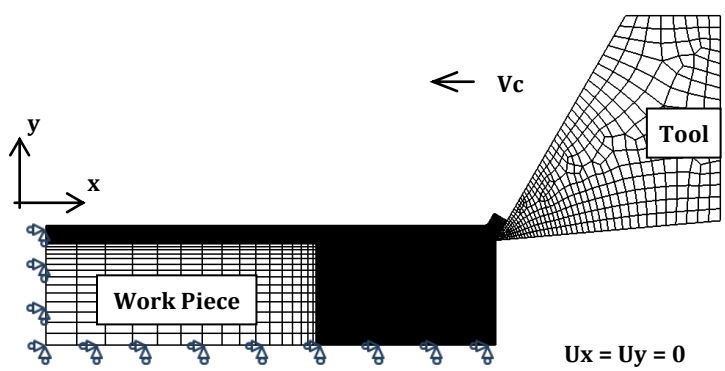

Figure 24: Finite element model

The work piece was modeled in three parts: chip, parting layer, and uncut material, as shown in Figure 25. The work piece was given the modified properties of 4340 steel. In addition, the parting layer elements were given failure parameters. As the strain in the

parting layer elements reached 1, due to the cutting action of the tool, the element failed and was removed from the calculation. This simulated the chip formation.

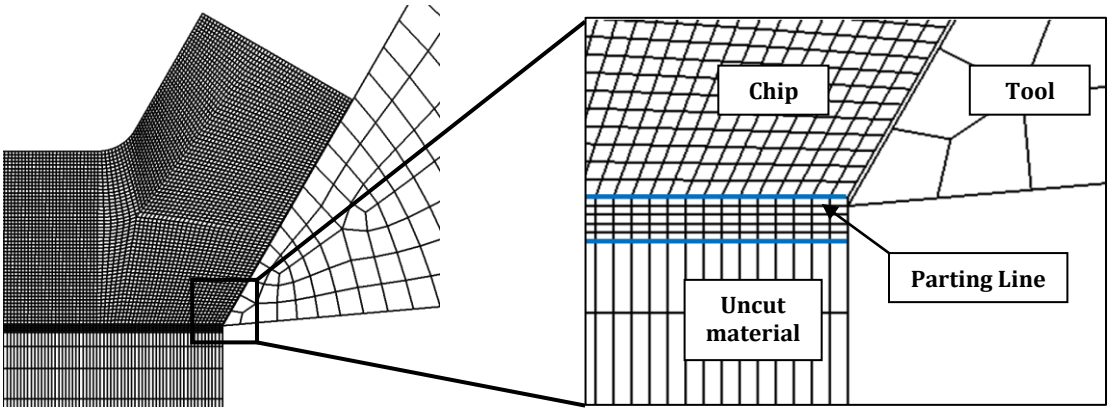

Figure 25: Closer view near the tool

The initial geometry of the chip was modeled similar to the geometry of the formed chip to prevent the squishing of elements above the parting line when the tool makes contact with the chip for the first time. The length of the work piece was 3,000 μm and modeled with a gradient mesh containing element sizes between 2 μm and 200 μm. Since the cutting speed was high, the simulation reached steady state within few a μm's of cut. Therefore, the initial length of the work piece (1,200 μm) was modeled with smaller elements (2 μm), and the remainder of the work piece was modeled with coarser elements to reduce the computational time.

4.2 Process of Shear Banding

The plots in Figure 11 show the rate of change of effective plastic strain between the bands during the cutting action of the tool. These plots also show the change in the shear angle between one formed shear band to the next. Figure 26(a) shows a completely formed shear band from the tool tip to the free surface of the chip. It should be noted that the band is narrow along the PSZ. As the tool moves, the band starts to become wider which are

shown in the Figure 26(b) and (c). Figure 26(d) shows the starting of a new shear plane angle. Then the shear bands follow the new shear plane angle and forms the next band which are shown in sequence in Figure 26(e) to (j).

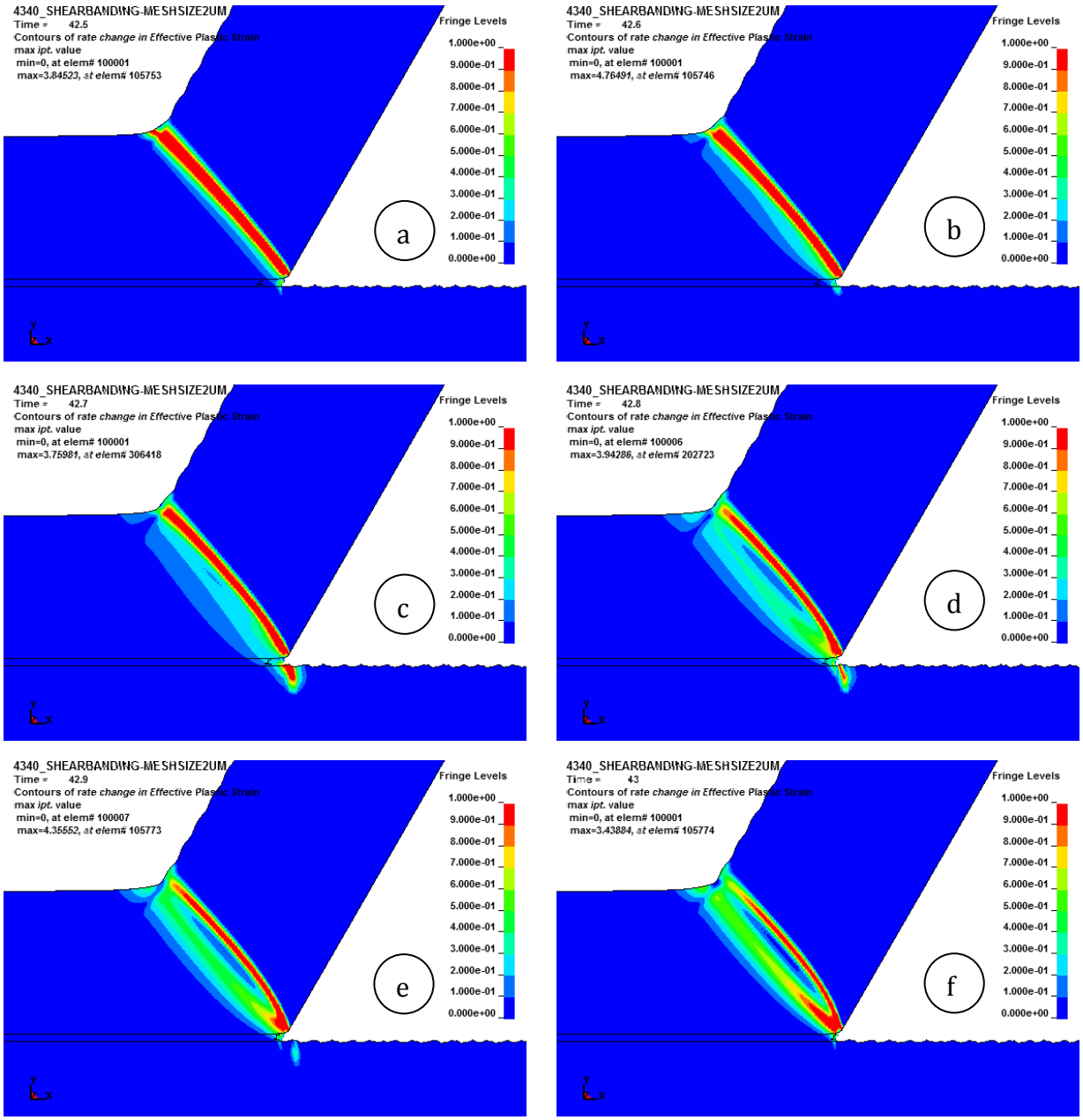

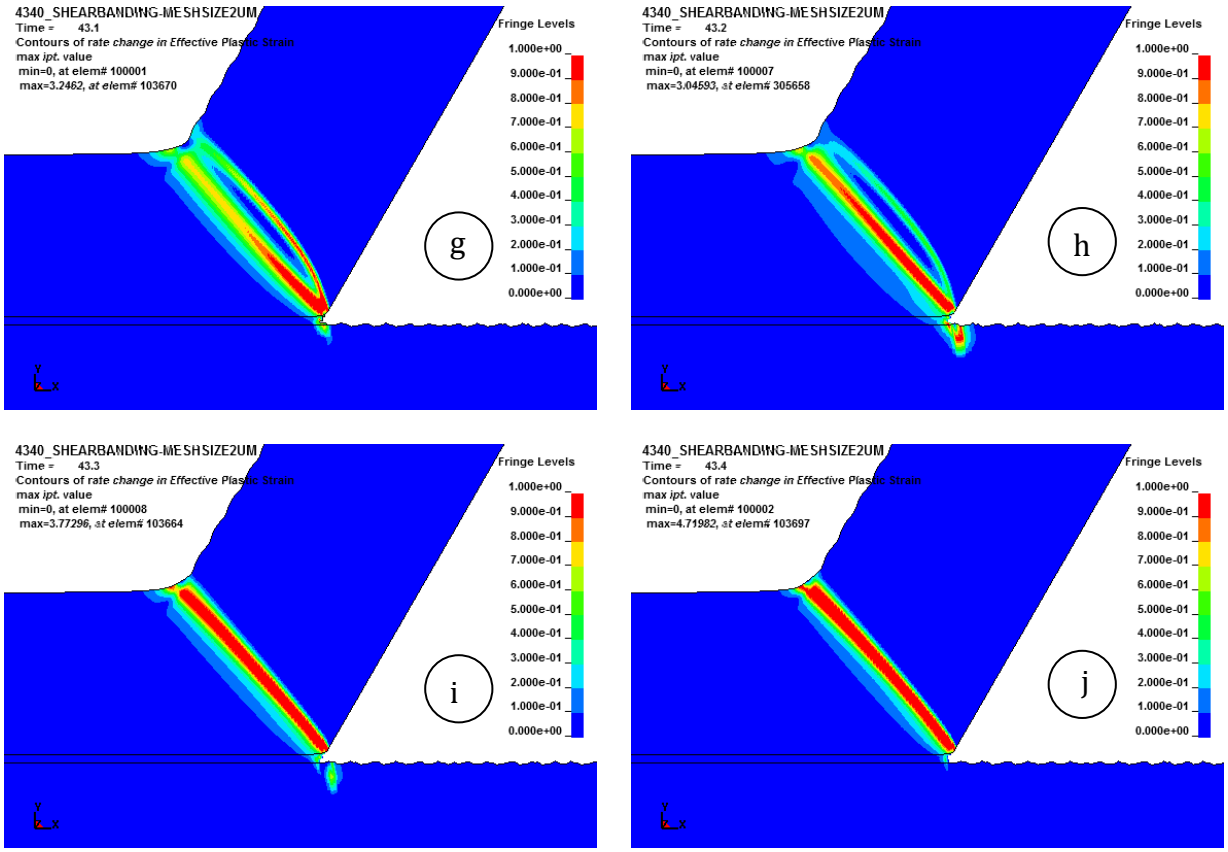

Figure 26: Sequence of ten images showing rate of change of effective plastic strain and change in shear plane angle between one formed band to next

4.3 Data Processing: Shear Band Spacing

Shear bands can be characterized by the strain values along the length of the chip. Figure 27 shows the plastic strain plot at steady state. The strain data was extracted along the CD direction starting from the PSZ up to 10 shear bands or 200 μm along the length of the chip. Enough data points were collected along the line so that strain values along the length of the chip were not overlooked.

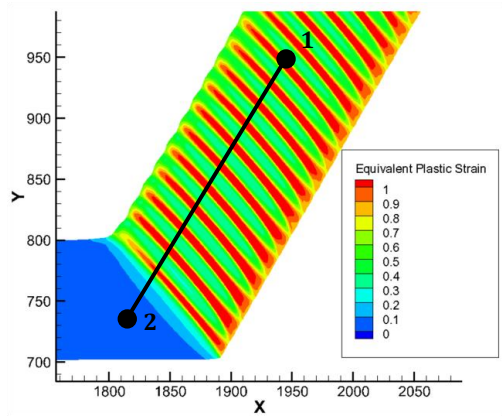

Figure 27: Plastic strain in the material at steady state condition

Figure 28 shows the plastic strain data along the length of the chip. The strain is zero below the PSZ, which corresponds to point 1 in Figure 27. As the material entered into the PSZ, the strain started to increase and then remained constant, as shown in the graph. Shear band spacing (Δ) can be measured between either the two peaks or the two valley points in the graph, as shown in the Figure 28. The spacing between the bands can also be measured by the ratio of maximum strain to the minimum strain.

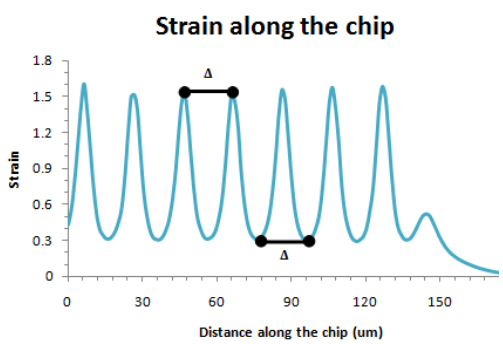

Figure 28: Plastic strain along the length of the chip

4.4 Results and Discussion

This section presents results of the parametric study of cutting parameters and physical properties of the material. Table 2 shows the different test conditions and their success.

Table 4 Cutting Conditions

No.	*DOC*	*Length*	*Tool*	*V_c (m/s)*	*μ*	*A (MPa)*	*B (MPa)*	*C*	*n*	*m*	*Tm (deg C)*	*Result*
1	100	3000	Rigid	30	0.1	226	792	1e-7	0.3	0.3	400	S
2	***50***	3000	Rigid	30	0.1	226	792	1e-7	0.3	0.3	400	S
3	***150***	3000	Rigid	30	0.1	226	792	1e-7	0.3	0.3	400	F
4	100	***6000***	Rigid	30	0.1	226	792	1e-7	0.3	0.3	400	S
5	100	3000	***Elastic***	30	0.1	226	792	1e-7	0.3	0.3	400	S
6	100	3000	Rigid	30	***0.2***	226	792	1e-7	0.3	0.3	400	F
7	100	3000	Rigid	30	***0.3***	226	792	1e-7	0.3	0.3	400	F
8	100	3000	Rigid	30	***0.4***	226	792	1e-7	0.3	0.3	400	F
9	100	3000	Rigid	30	***0.5***	226	792	1e-7	0.3	0.3	400	F
10	100	3000	Rigid	30	0.1	226	792	1e-7	***0.1***	0.3	400	F
11	100	3000	Rigid	30	0.1	226	792	1e-7	***0.2***	0.3	400	F
12	100	3000	Rigid	30	0.1	226	792	1e-7	***0.4***	0.3	400	S
13	100	3000	Rigid	30	0.1	226	792	1e-7	***0.5***	0.3	400	S
14	100	3000	Rigid	30	0.1	226	792	1e-7	0.3	***0.1***	400	S
15	100	3000	Rigid	30	0.1	226	792	1e-7	0.3	***0.2***	400	F
16	100	3000	Rigid	30	0.1	226	792	1e-7	0.3	***0.4***	400	F
17	100	3000	Rigid	30	0.1	226	792	1e-7	0.3	***0.5***	400	F
18	100	3000	Rigid	30	0.1	226	792	1e-7	0.3	0.3	***200***	F
19	100	3000	Rigid	30	0.1	226	792	1e-7	0.3	0.3	***300***	F
20	100	3000	Rigid	30	0.1	226	792	1e-7	0.3	0.3	***500***	S
21	100	3000	Rigid	30	0.1	226	792	1e-7	0.3	0.3	***600***	S

S – Successful completion of simulation
F – Simulation crashed due to excessive mesh distortion

4.5 Effect of Cutting Condition Parameters

4.5.1 Effect of Depth of Cut

The change in the depth of cut significantly affected the strain values along the length of the chip. There was not much oscillation in the strain values along the length of the chip for the simulation with the DOC of 50 μm. With 150 μm as the DOC, the simulation crashed after forming two bands, due to heavy plastic deformation. Figure 29 shows the plots of plastic strain along the length of the chip. Figure 30 shows the variation of the

shear band spacing with the increase in the depth of cut. It can be seen from the plots that as the depth of cut increases, the chances of the formation of shear bands are higher.

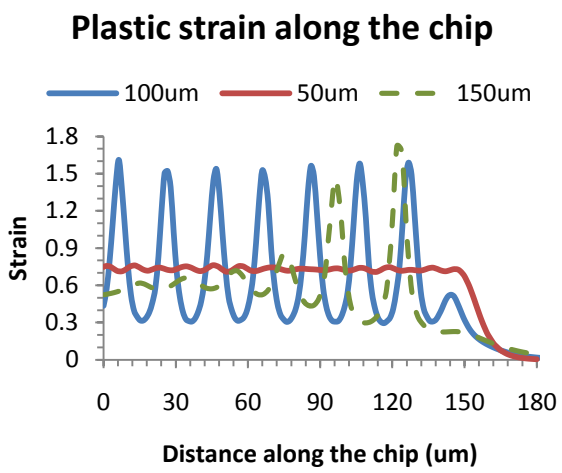

Figure 29: Plastic strain along the length of the chip– Effect of depth of cut

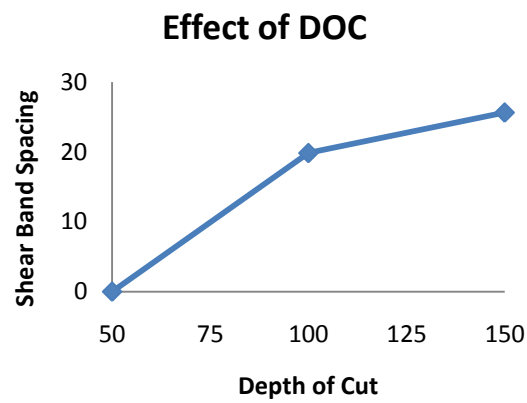

Figure 30: Shear band spacing—effect of depth of cut

4.5.2 Effect of Length of Work Piece and Elastic Tool

The change in the length of the work piece significantly affected the strain values along the length of the chip. Figure 31 shows the plastic strain data for the different lengths of the work piece and the elastic tool. The oscillation in the strain values along the length of the chip was less for the simulation involving the work piece length of 6,000 μm versus the workpiece of length 3,000 μm.

The shear band spacing for the simulations, shown in Figure 32, increased when the tool became elastic. This might be due to the effect of tool oscillation on the cutting forces rather than being rigid. There was no shear banding seen with the increase in length of the work piece.

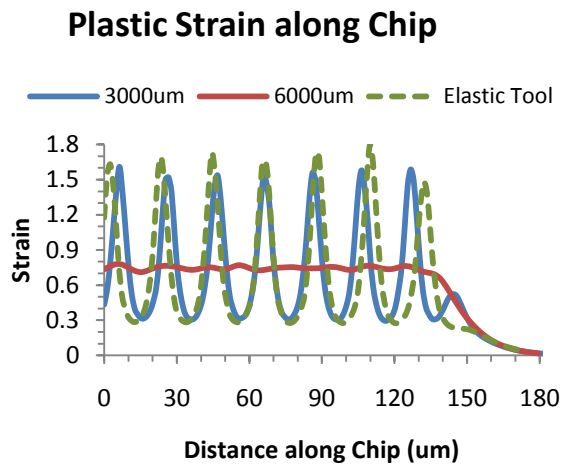

Figure 31: Plastic strain along length of chip—effect of length of work piece and elastic tool

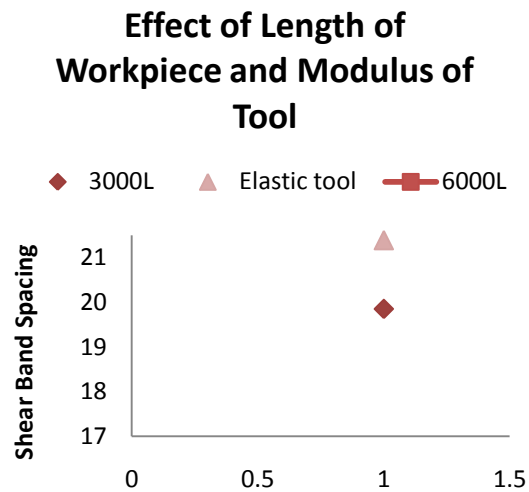

Figure 32: Shear band spacing—effect of length of work piece and elastic tool

4.5.3 Effect of Friction

The change in friction between the tool and work piece did not result in successful completion of the simulations. Simulations were run for different values of friction from 0.1 to 0.5. The simulations with a friction coefficient above 0.1 was not completed because the chip elements got squished and entered into negative volume when the tool made initial contact with the work piece. Figure 33 and Figure 34 show the plastic strain variation and shear band spacing for all the values of the friction coefficient.

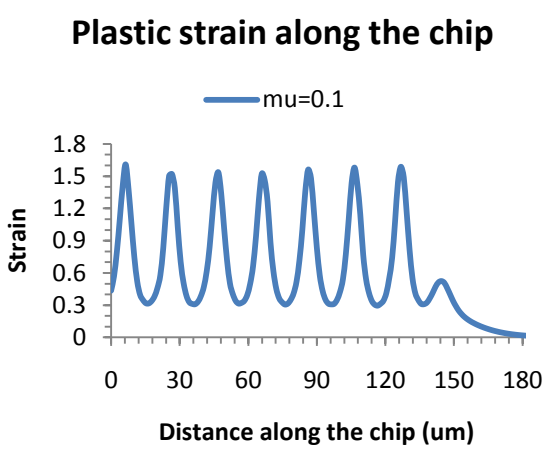

Figure 33: Plastic strain along the length of the chip – Effect of friction

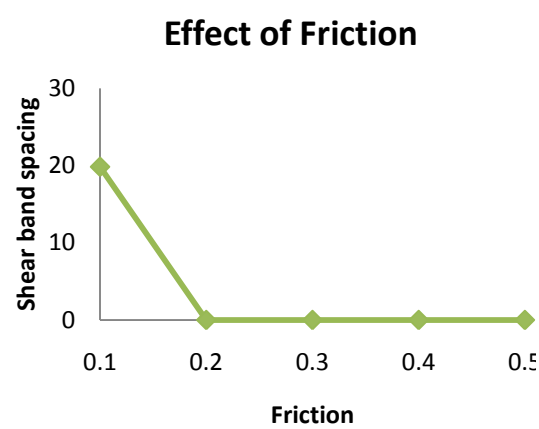

Figure 34: Shear band spacing—effect of friction

4.5.4 Effect of Work Hardening

Simulations were performed for the five different values of work-hardening coefficients from 0.1 to 0.5. Of the five simulations, two were successful, and the simulations with 0.1 and 0.2 as the work hardening coefficients failed after one narrow shear band because of the lack of strength in the material. Figure 35 shows the plastic strain plots for different values of work hardening. The simulations with 0.1 and 0.2 as the work-hardening parameter failed after forming a few narrow shear bands. The reason for narrow shear band was smaller value of n lesser the flow stress which increases the chance of localization. With 0.4 and 0.5 as the work-hardening coefficients, the strength of the material was increased and produced a thicker chip. Since the flow stress was higher, the strain data showed fewer oscillations along the length of the chip. From Figure 36 it can be seen that as the work hardening increased, the chances of shear banding decreased.

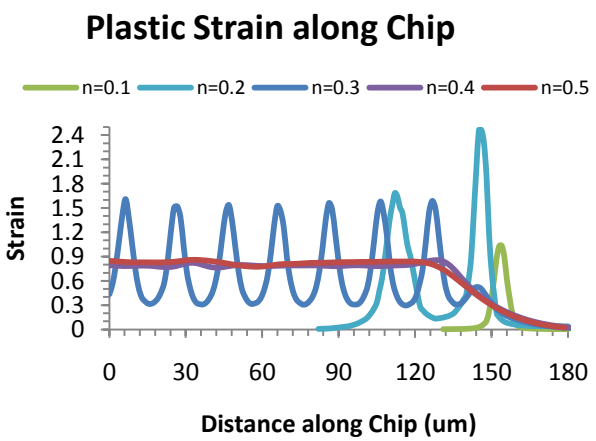

Figure 35: Plastic strain along length of chip—effect of work hardening

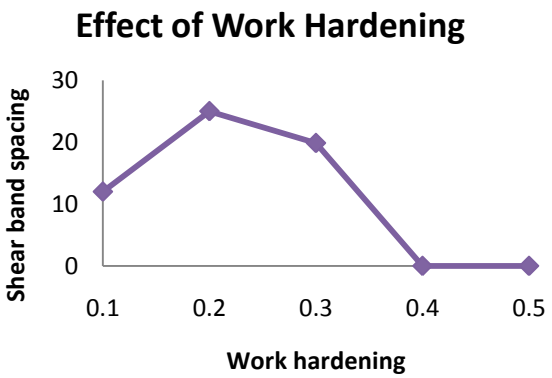

Figure 36: Shear band spacing—effect of work hardening

4.5.5 Effect of Thermal Softening

The fifth parameter variation was the thermal softening coefficient m. Five different values were chosen for m in the simulations: 0.1, 0.2, 0.3, 0.4, and 0.5.

Figure 37 shows the plastic strain data for two different values of m, namely 0.1 and 0.3. Fewer oscillations were seen in the strain values along the length of the chip for the simulation with m = 0.1. At higher values of m (m = 0.4 and 0.5), the chip material protruded out of the tool due to heavy plastic deformation. Since the flow stress was also higher at m = 0.4 and 0.5, no shear bands were seen along the length of the chip. The shear band spacing for different values of the thermal softening parameter is shown in Figure 38.

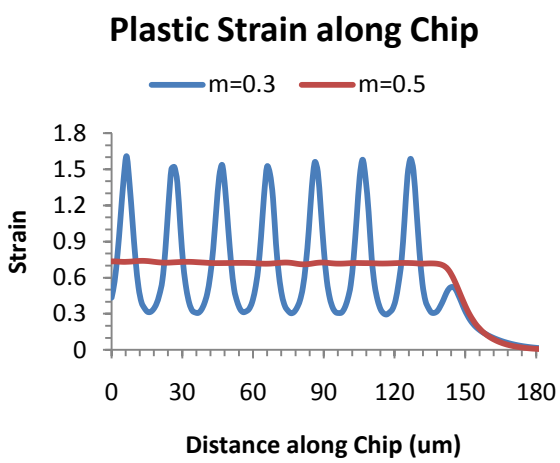

Figure 37: Plastic strain along length of chip—effect of thermal softening

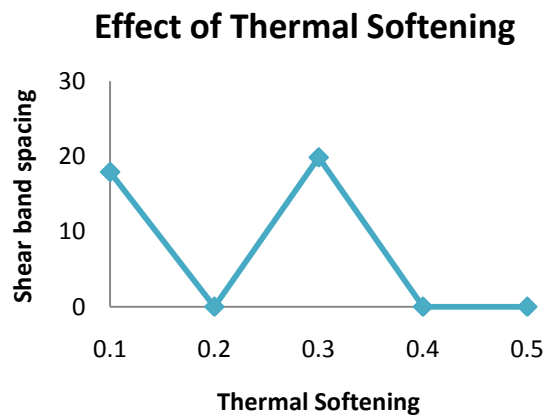

Figure 38: Shear band spacing—effect of thermal softening

4.5.6 Effect of Melting Temperature

The computed melting temperature value of the material was 400 deg C. The melting temperature was varied between 200 deg C and 600 deg C. Figure 39 shows the plastic strain along the chip for different melting temperatures. The simulation at 200 deg C for the melting temperature crashed because the work piece was behaving as a fluid with much lower flow stress and not able to handle huge plastic deformation, which is required for stress localization. As the melting temperature increased, the chances of shear banding

decreased (Figure 40). This is because the flow stress was higher with the melting temperature being high, so the tendency to stress localization decreased.

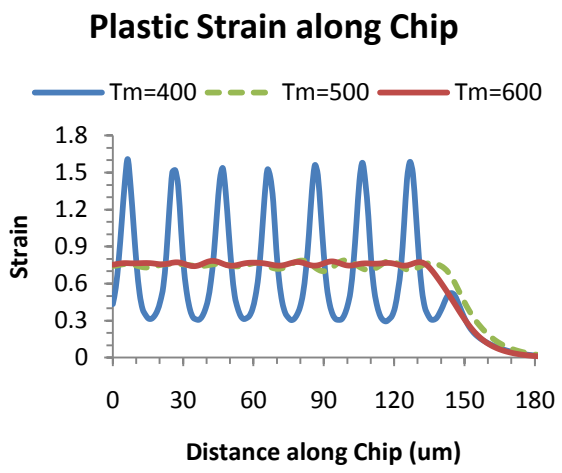

Figure 39: Plastic strain along length of chip—effect of melting temperature

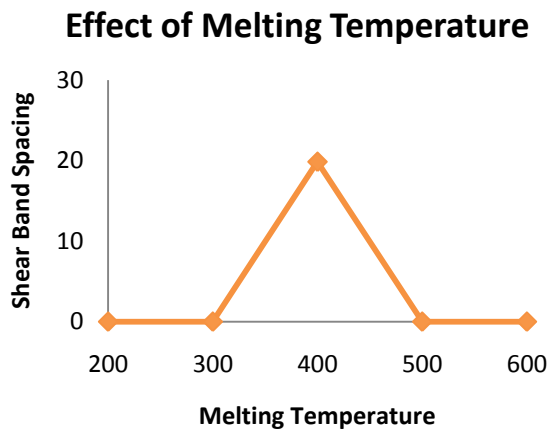

Figure 40: Shear band spacing—effect of melting temperature

CHAPTER 5

CONCLUSIONS AND FUTURE WORK

5.1 Conclusions

5.1.1 Simulations results from ABAQUS

A user material property that includes the effect of thermal softening for 4340 steel at 18 HRC was computed using MAPLE from the original properties given by Johnson and Cook (1984). ALE approach is used to simulate high-speed machining simulations with no damage properties given to the elements. Finite element results showed shear banding for one cutting condition with mass scaling and smooth chip formation was seen when the mass scaling was removed.

Finite element studies in literature that showed the formation of adiabatic shear banding in a FE package DEFORM using strain softening was reproduced in ABAQUS under same cutting conditions and material model. Results showed adiabatic shear banding after varying the adaptive mesh controls parameters.

The following are the results of the simulations.

- ALE approach in ABAQUS did not produce the same chip geometry shown in literature because the simulations failed since the mesh was not able to reform to a large extent and produce concave shapes as we see in serrated chips
- Mass scaling with a factor of 100 did not affect the result
- Mesh size needs to be small to capture the strains correctly. The strain seems to diffuse with the increase in the element size
- The parameter controlling curvature based refinement was reduced to simulate shear banding successfully

- Increase in the value of parameter "M" in the material model (4) decreased the peak strain in PSZ.

5.1.2 Simulations results from LS Dyna

A user material property that includes the effect of thermal softening for 4340 steel at 18 HRC was computed using MAPLE from the original properties given by Johnson and Cook (1984). High-speed machining simulations were performed by varying the cutting parameters by Lagrangian approach with damage parameters given to parting line elements to simulate chip formation. Results showed shear banding for a few cutting conditions and for most it crashed due to severe plastic deformations. Therefore, this approach is not suitable for predicting the occurrence of shear bands.

5.2 Future Work

In the future, a realistic plot of PEEQ vs Edot could be used in the MAPLE file to predict new constants of the JC model and perform simulations in order to understand the occurrence of shear bands.

BIBLIOGRAPHY

BIBLIOGRAPHY

Aurich, J. C., and Bil, H., 2006, 3D finite element modeling of segmented chip formation. *CIRP Annals—Manufacturing and Technology*, 55, pp. 47-50.

Belhadi, S., Mabrouki, T., Rigal, J. F., and Boulanouar, L., 2005, Experimental and numerical study of chip formation during straight turning of hardened AISI 4340 steel. *Proceedings of the Institution of Mechanical Engineers. Part B. Journal of Engineering Architecture,* 219, pp. 515-524.

Bäker, Martin, 2003, An investigation of the chip segmentation process using finite elements. *Technische Mechanik,* 23, pp. 556-562.

Bäker, Martin, Rosler, Joachim, and Siemers, Carsten, 2003, The influence of plastic properties on chip formation. *Computational Material Science,* 28, pp. 556-562.

Davies, T. J., and Burns, M. A., 2002, On repeated adiabatic shear band formation during high-speed machining. *International Journal of Plasticity.* 18, pp. 487-506.

Duan, C. Z., Dou, T., Cai, Y. J., and Li, Y. Y., 2009, Finite element simulation and experiment of chip formation process during high speed machining of AISI 1045 hardened steel. *International Journal of Recent Trends in Engineering,* 1, pp. 46-50.

Ng, Eu-gene, and Aspinwall, K. David, 2002, Modeling of hard part machining. *Journal of Materials Processing Technology*, 127, pp. 222-229.

Guo, Y. B., and Wen, Q., 2005, A hybrid modeling approach to investigate chip morphology transition with the stagnation effect by cutting edge geometry. *Transactions of NAMRI/SME,* 33, pp. 469-476.

Guo, Y. B., and Yen, W. David, 2004, A FEM study on mechanisms of discontinuous chip formation in hard machining. *Journal of Materials Processing Technology,* 155-156, pp. 1350-1356.

Johnson, R. Gordon, and Cook, H. William, 1985, Fracture characteristics of three metals subjected to various strains, strain rates, temperatures and pressures. *Fracture Mechanics*, 21, pp. 31-48.

Karpat, Y., 2010, A modified material model for the finite element simulation of machining titanium alloy Ti-6Al-4V. *Machining Science and Technology,* 14, pp, 390-410.

Ozel, Tuğrul, and Sima, Mohammed, 2010, Finite element simulation of high speed machining of Ti-6Al-4V alloy using modified material models. *Transactions of NAMRI/SME,* 38, pp. 48-56.

Recht, R. F., 1964, Catastrophic thermoplastic shear. *Journal of Applied Mechanics,* 86, pp. 189-193.

BIBLIOGRAPHY (continued)

Uhlmann. E., Graf von der Schulenberg, M., and Zettier, R., 2007, Finite element modeling and simulation of Inconel 718. *CIRP Annals,* 56, pp. 61-64.

Xie, J. Q., Bayoumi, A. E., and Zbib, H. M, 1998, FEA modeling and simulation of shear localized chip formation in metal cutting. *International Journal of Machine Tools and Manufacture,* 38, pp. 1067-1087.